CHALMERS
UNIVERSITY OF TECHNOLOGY

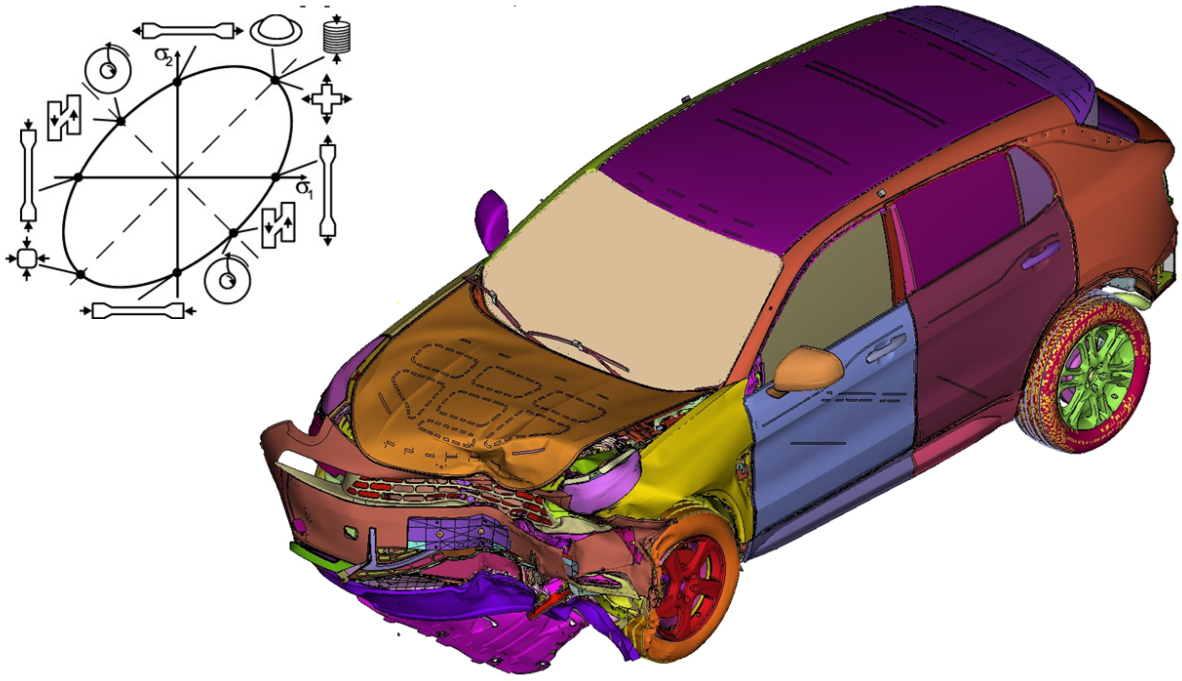

Material models and crash simulations in LS-DYNA

Development of virtual test laboratory

Master's thesis in Automotive Engineering

MAYUR SUDARSHAN RAO
SRIHARSHA SHANKAR RAO VISWANATH

Department of Mechanics and Maritime Sciences
CHALMERS UNIVERSITY OF TECHNOLOGY
Gothenburg, Sweden 2021

Master's thesis 2021:04

Material models and Crash simulation in LS-DYNA

Development of virtual test laboratory

MAYUR SUDARSHAN RAO
SRIHARSHA SHANKAR RAO VISWANATH

CHALMERS
UNIVERSITY OF TECHNOLOGY

Department of Mechanics and Maritime Sciences
Division of Vehicle Safety
Chalmers University of Technology
Gothenburg, Sweden 2021

Material models and crash simulations in LS-DYNA
Development of virtual test laboratory
MAYUR SUDARSHAN RAO
SRIHARSHA SHANKAR RAO VISWANATH

Manager: Dag Thuvesen, Safety-CAE, CEVT AB
Supervisors: Hans Merkle, Safety-CAE, CEVT AB
Martin Larsson, Safety-CAE, CEVT AB
Examiner: Robert Thomson, Division of Vehicle Safety, Chalmers University

Master's Thesis 2021:04
Department of Mechanics and Maritime Sciences
Division of Vehicle Safety
Chalmers University of Technology
SE-412 96 Gothenburg

Cover: Offset Deformable Barrier (ODB) crash test showing deformation of front end of the vehicle along with the yield locus showing different stress states.

Gothenburg, Sweden 2021

Material models and crash simulations in LS-DYNA
Development of Virtual test laboratory

MAYUR SUDARSHAN RAO
SRIHARSHA SHANKAR RAO VISWANATH
Department of Mechanics and Maritime Sciences
Division of Vehicle Safety
Chalmers University of Technology

Abstract

Extensive developments in the field of computational mechanics led to substantial improvements in the assessment of vehicles in a virtual environment. Vehicle safety is one of the prime areas where virtual simulations are comprehensively used in the product development phase. In order to obtain effective results, it is very important that the material model predicts the failure behaviour accurately in crash analysis. The main goal of the current study is to contribute to the development of a virtual material test laboratory where different materials can be tested in multiple stress states in LS-DYNA using a calibrated input flow curve (obtained from an uniaxial tension test simulation).

The study was carried out in two phases. Initially, coupon tests were simulated using solid fine elements which were finally validated against the experimental results in order to achieve better accuracy. A input flow curve was calibrated from the uniaxial tension test simulations using optimisation technique and the same curve was finalized for all the further simulations. The same coupon tests were then simulated using shell elements and a damage model (GISSMO) was coupled to a constitutive material model, as damage models play an important role in predicting the fracture in the material. Necessary information like triaxiality values, failure strain, and critical strains computed from the solid element models was used to calibrate the GISSMO model. The calibrated model was then subjected to mesh regularization for element sizes varying from 0.5mm to 5mm to determine the sensitivity of mesh size on failure prediction.

The calibrated material model for shells showed promising results and was in good agreement with experiments and in a full scale Offset Deformable Barrier crash simulation. The material model was computationally efficient and, using this methodology, different stress states can be predicted quite effectively using a single flow curve (derived from simple tension test). This methodology can also be verified for other metals and polymers.

Keywords: LS-DYNA,*MAT_024, GISSMO, Optimisation, triaxiality, critical strain, failure strain,flow curve.

Acknowledgement

This Master Thesis was carried out at China Euro Vehicle Technology (CEVT) at Gothenburg, in cooperation with the division of vehicle safety, Mechanics and Maritime sciences department at Chalmers University of Technology. We would like to thank Dag Thuvesen, Senior manager - Safety CAE at CEVT for giving this opportunity and all the necessary resources to complete the project.

Sincere thanks to our supervisors Hans Merkle and Martin Larsson, Senior CAE engineers, for their immense support, guidance and sharing knowledge through out the thesis work. Special thanks to our examiner Prof. Robert Thomson at Chalmers University for his feedback, help and valuable support during the project.

We would like to extend our gratitude to Mikael Schill and David Aspenberg at Dynamore Nordic for their help and support in calibrating the damage model. We finally extend our gratitude to the entire Safety CAE team at CEVT for their support and for making our stay a memorable one.

Mayur Sudarshan Rao
Sriharsha Shankar Rao Viswanath
Gothenburg, December 2020

Contents

List of Figures

List of Tables

NOMENCLATURE

CAE - Computer Aided Engineering

PD - Product Development

NVH - Noise Vibration and Harshness

BIW - Body in White

HSS - High strength steels

HSLA - high strength low alloy steels

DP - Dual Phase

SRSM - Successive Response Surface Method

MDO - Multidisciplinary optimisation

FEM - Finite Element Method

DOF - Degree Of Freedom

FE - Finite Element

DIEM - Damage Initiation and Evolution Model

GISSMO - Generalized Incremental Stress-State dependent damage MOdel

OEM - Original Equipment Manufacturer

ELFORM - Element Formulation

1
Introduction

The adaptation of CAE in product development procedures has resulted in remarkable reductions in design factors and accelerated the process of developing several design concepts with different configurations. The need for extensive physical experiments were reduced and calculations using numerical techniques helps model the physical experiments on the virtual platform. Advancements in CAE has brought about decreased need for prototype samples, reductions in weight, and provides realistic visualisations [1].
Use of CAE in the automotive industry is found in several departments like vehicle integration, energy systems, powertrain, body, suspension systems, etc. Structural analysis involving crash simulations, NVH, and durability analysis [2] is particularly suitable for CAE. Various CAE methods and methodologies have been implemented to calculate field variables like deformations, stresses, and energies (eg. strain energy, potential energy etc.).
During recent times, the study of vehicle impact behaviour by virtual methods has gained importance. Crash test simulation has been used to optimise the behavior of the structures involved in a collision. Requirements for safety guidelines are reported in the literature by analysing the energies (strain energy and kinetic energy) and structural deformations with crash test simulations. Mapping experimental results in a realistic manner with CAE, provides an understanding of engineering materials and their behaviour. The transformation of kinetic energy of the vehicle into deformation of the car body can be studied computationally and correlated with experimental test results [3].
The most conventionally used material in the automotive sector (specially for Body in White) is steel. There has been a preference for usage of steel in the past century because of its wide range of yield strengths with high modulus of elasticity. The compliant properties of steel in terms of resistance to corrosion, formability, etc., has made steel an inevitable part of an automotive industry.
The new generation of steels have reinforced its rampant use due to improved structural strength. According to the International Organisation of Motor Vehicle manufacturers, around 95 million vehicles were rolled out in the year 2018 [4] and this report also highlighted the usage of new generation high strength steels and advanced high strength steels. Around 34% of new age steels were found to be incorporated in BIW, while use in suspension systems comprised 12% - 17% of modern steels. The introduction of new grade steels has resulted in reductions of total weight of the vehicle leading to reduced fuel consumption and 15 % lower CO_2 life cycle emissions. Aditionally, the new grade steels have enabled engineering of advanced crash resistant structures [5].

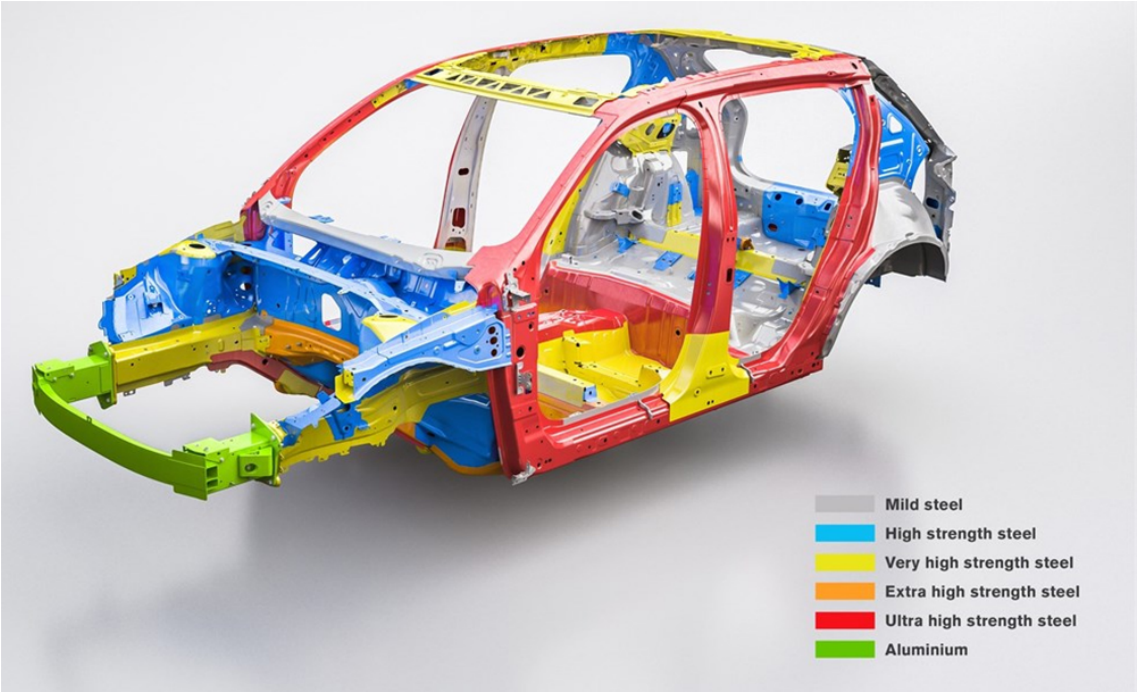

Figure 1.1: BIW of a car (Image from Google Images)

Based on available models, the variability of material properties and other conditions cannot be mapped consistently and this has led to indeterministic models [6]. Hence, the demand for precise material behaviour and material failure under different stress states, strain rates, etc., have been found to be important and this requires extensive experimental test results [7].
To calibrate a virtual material model, experimental test results (representing different multi-axial stress state behaviour) have been reported in the literature. The main objective of this thesis was to contribute to the development of a virtual material test laboratory. China Euro Vehicle Technology (CEVT), a major research and development center in Sweden, has implemented the MFGenYld+CrachFEM material model (commonly known as CrachFEM material model) for their simulations involving structural analysis. This material model (developed by MATFEM) has been based on the failure criteria of the material. These CrachFEM material models have versatile failure modelling capabilities using a phenomenological approach. However these models have a high computational cost with an additional licensing expenditure.
The primary focus of the current work is to study the comprehensive material behaviour of Dual Phase steel can be captured in uniaxial tensile test through simulation. Here the material is assumed to be isotropic, homogeneous and free from residual stresses. In this thesis the material model developed is focused on the experimental tensile test results.

2

Theory

2.1 Explicit and Implicit Time Integration

Numerical methods are one of the powerful tools or techniques which play an important role in solving higher order differential equations (used to define complex systems involving multi degrees of freedom). Finite element analysis use this numerical approximation techniques to solve the higher order equations. Finite element analysis is majorly classified into two types i.e. static analysis and dynamic analysis. In static analysis, there is no effect of mass (inertia) or damping. In dynamic analysis, nodal forces associated with mass/inertia and damping are included. Dynamic analysis involves solving the equations using either explicit or implicit time integration [20].

Implicit finite element methods deal with the technique of inverting the stiffness matrix at each and every step for a given load step. Diagonality of matrix, after inversion is lost for complex systems involving multi degrees of freedom, while explicit analysis accomodates nonlinearities with sub stepping algorithms which are further subdivided into infinitesimal increments.

The explicit method implies that instead of solving for u it solves for ü. Yang et al. [19] claims that this is an advantage because solving the inverse could be computationally demanding when considering large systems involving higher order differential equations.

In the Crank Nicolson method, the second order derivative at time step n+1 is defined by,

$$\boldsymbol{M}\ddot{u}_{n+1} + \boldsymbol{C}\dot{u}_{n+1} + \boldsymbol{K}u_{n+1} = \boldsymbol{P}_{n+1} \tag{2.1}$$

Where $\boldsymbol{M}$ is the mass matrix, $\boldsymbol{C}$ is the damping coefficient, $\boldsymbol{K}$ is the stiffness matrix, ü is the acceleration, u̇ is the velocity, u is the displacement, n is the current time step where the nodal values are determined.

First order derivative is expanded as:

$$\dot{u}_{n+1} = \dot{u}_n + \frac{h^2}{4}[\ddot{u}_n + \ddot{u}_{n+1}] \tag{2.2}$$

While 0^{th} order derivative uses,

$$u_{n+1} = u_n + h\dot{u}_n + \frac{h^2}{4}[\ddot{u}_n + \ddot{u}_{n+1}] \tag{2.3}$$

For n=0, ü is obtained from,

$$\ddot{u}_0 = M^{-1}(p_0 - C\dot{u}_0 - Ku_0). \tag{2.4}$$

According to Equations 2.2 and 2.3, an equation system for ü is obtained in terms of $\dot{u}_n$ and & u_n.

The time step size (h) is bounded by the largest natural frequency of the structure which in turn is bounded by the highest frequency of any individual element in the FE mesh.

2.2 Steels

Dual phase steels are one of the important variants of high strength steels which are comprised of a ferrite matrix and dispersed phase of martensite/restained austenite and/or bainite. Development of these DP steels has resulted in steel grades with high tensile strength and elongation properties to establish fatigue and crash resistance. Cold rolling of low alloy steels followed by inter critical annealing are one of the widely accepted methods to produce DP steels. These steels are mainly used in the body panels, wheels, B pillars, bumpers and other important automotive components.
Advantages of DP steels are as follows:

- Low yield strength
- High strain sensitivity
- Good fatigue resistance
- High deformation hardening that leads to high energy absorbing ability (Crashworthiness).

2.3 Strain rate sensitivity

The phenomenon of non-linear increase in stress when a material is subjected to an increasing strain rate corresponds to strain rate sensitivity. This behaviour is observed in a wide range of metals. Usually it is governed by,

$$\sigma_f = k\dot{\varepsilon}^m \tag{2.5}$$

where σ_f is flow stress, $\dot{\varepsilon}$ is strain rate, k is a constant and 'm' represents the strain rate sensitivity (varies with temperature and grain size)

2.4 Constitutive modelling

To characterise the behaviour of a material, a number of idealised responses are required [12]. Mechanical analysis of engineering materials and their behaviour in indeterminate structures cannot be easily assessed which led to the development of constitutive models that help in linking states of stress and strain. From a

mathematical viewpoint, the constitutive equations (that defines the constitutive model) are complementary equations to balance kinematic equations. The constitutive equations coupled with the equilibrium equations and kinematics of the boundary conditions leads to the formulation a of complete boundary value problem.

Constitutive models vary for the different materials used in engineering practice, such as metals and alloys, polymers, fiber composites (with polymer or metal matrix), concrete and wood. The mechanical properties are often significantly affected by the temperature and by the loading rate. Plastic behaviour is characterised by irreversible strains when the material reaches a yield stress limit [16]. Modelling of plasticity is based on a yield criterion, flow rule and hardening rule [9].

2.4.1 Yield Criterion

A yield criterion is defined as a hypothesis that defines the elastic limit of the material (maximum extent of the material that can withstand the load without permanent changes in the size or shape) and a yield criterion also describes the genesis of plastic deformation under the action of external loads. A stress value within the limits of the surface yields elastic strains.

Commonly used yield criteria for metals are von Mises yield criterion as shown in Figure 2.1 and Tresca yield criteria as shown in the Figure 2.2 [9].

The yield surface is defined by the yield criterion that a material undergoes during deformation. Stress invariants or three dimensional principal stresses are typically used to determine the shape of the yield or yield surface.

$$f(\sigma_1, \sigma_2, \sigma_3) = 0 \tag{2.6}$$

where σ_i = Principal stresses

$$f(I_1, J_2, J_3) = 0 \tag{2.7}$$

where I_1 = First invariant of cauchy stress
= Sum of stresses along the principal axes
= $\sigma_1+\sigma_2+\sigma_3$
J_2, J_3 = Second and third principal invariants of deviotoric part

Predominant theories used in engineering that define yield surfaces are as follows:

1. **von Mises surface**

This theory is based on the assumption that yield of the material begins when the principal stresses induced in the material satisfies the following relation:

$$\sigma_y = \sqrt{(\frac{3}{2})}\sqrt{(\sigma_1 - \sigma_m)^2 + (\sigma_2 - \sigma_m)^2 + (\sigma_3 - \sigma_m)^2} \tag{2.8}$$

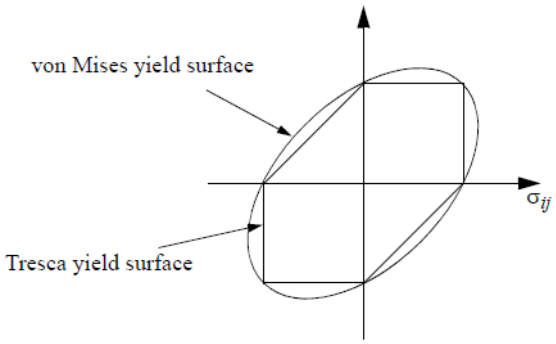

Figure 2.1: Von mises and Tresca yield criterion in σ_1 and σ_2 [8]

2. **Tresca yield surface**
This theory is based on the assumption that yield of the material begins when the maximum shear stress in the material attains a critical stress.

$$max(|\sigma_1 - \sigma_2|, |\sigma_2 - \sigma_3|, |\sigma_3 - \sigma_1|) - \sigma_f = 0 \tag{2.9}$$

where σ_f = Flow stress

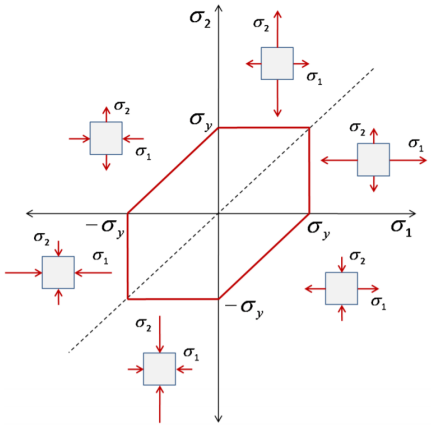

Figure 2.2: Tresca yield surface [8]

2.4.2 Flow rule

The plastic behaviour of metals is described by a plasticity flow rule. It is used to characterise the amount of plastic deformation. Total strain can be decomposed into elastic and plastic strains. Elastic strains can be computed using constitutive models (hyperelastic model) while the plastic strain computation depends on a flow rule and hardening rule.

2.4.3 Hardening rule

A hardening rule used to define the evolution of yield surface during a deformation process. Usually, metallic materials increase their strength when subjected to

plastic deformation. Increase in yield strength lead to a change in the yield surface because the yield surface is a generalised term of yield strength. This phenomenon of subsequent transformation of yield surface (yielding behaviour) due to plastic loading is called the hardening rule [12]. Generally a hardening behaviour is predicted using phenomenological models while there are many other models like Bingham viscoplastic model, Maxwell rheological model, Perzyna's formulation etc. that also describes the behaviour of the material [17]. Based on the response of the yield surface during the plastic loading and elastic unloading, hardening behavior is often broadly classified into three main types namely

1. Isotropic hardening plastic behavior
2. Kinematic hardening plastic behavior
3. Distortional hardedning or Mixed isotropic and kinematic hardening plastic behavior

2.4.3.1 Isotropic hardening

An increased plastic deformation with an increase in yield stress of the material results in the uniform expansion of the yield surface from the original state that is referred to as hardening plasticity. Isotropic hardening rule states that when yield stress (during loading) is exceeded then the yield surface proportionally expands in all directions as shown in Figure 2.3 under isothermal conditions. As the hardening variable k changes due to plastic loading, size of the yield function (determined by the initial yield function) also changes. The plastic strain helps to recognise hardening model using uniaxial stress strain [8]. Yield function (ϕ) is expressed as:

$$\phi(\sigma, \kappa) = |\sigma| - (\sigma_y + \kappa) \tag{2.10}$$

where,

- κ = micro hardening stress or drag stress representing the hardening state of the microstructure of the material. = -Hk
- H = Hardening modulus that is associated with plastic strain and H>0
- k = internal hardening variable
- $|\sigma|$ = Applied load

The flow stresses are described as a function of equivalent plastic strain.

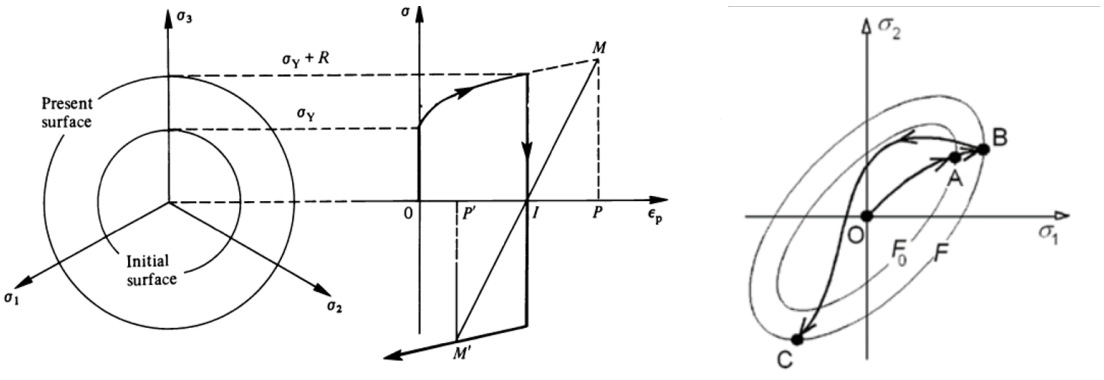

Figure 2.3: Isotropic hardening [8]

2.4.3.2 Kinematic hardening

Kinematic hardening states that when yield stress (during loading) is exceeded then the yield surface translates in the direction of the stress as seen in the Figure 2.4. Here the size and shape of the yield surface remains unaltered. As the hardening variable k changes due to plastic loading, shape of the yield function (determined by the initial yield function) also changes. This rule is applicable when a metal (particularly steels) experiences reversed loading [8]. Yield function (ϕ) is expressed as:

$$\phi(\sigma, \kappa) = |\sigma^{red}| - (\sigma_y) \tag{2.11}$$

where,

- $|\sigma^{red}| = \sigma$ - α
- α is back stress due to kinematic hardening.
- σ^{red} is reduced stresses.
- $|\sigma|$ = Applied load

The flow stresses are described as a function of equivalent plastic strain.

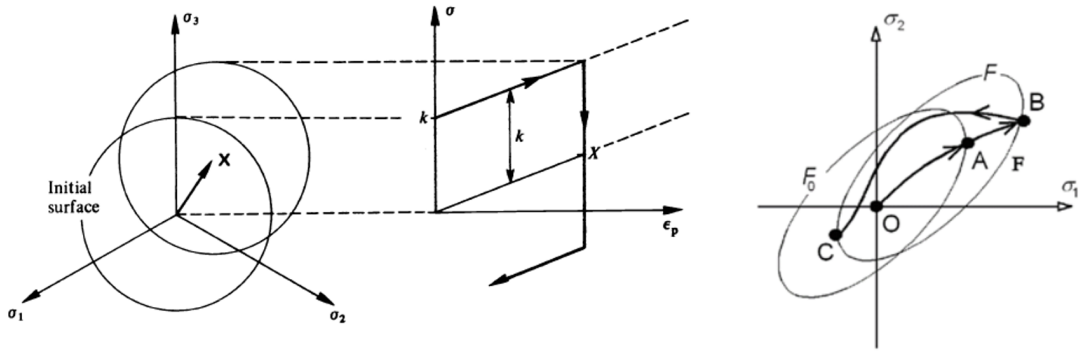

Figure 2.4: Kinematic hardening [8]

2.4.3.3 Mixed hardening or Distortional hardening

The combination of isotropic and kinematic hardening gives mixed hardening behaviour. Figure 2.5 shows the dislocation of the yield surface based on distortional hardening theory. The behaviour of the material under this rule refers to the distortion of yield surface during the course of plastic deformation coupled with other hardening rule [10]. This rule is generally applicable for modelling the behaviour of orthotropic materials. Loading/Yield function is expressed as:

$$\phi(\sigma, \kappa) = |\sigma^{red}| - (\sigma_y + \kappa) \tag{2.12}$$

where $|\sigma^{red}| = \sigma$ - α
κ is micro hardening stress due to isotropic hardening and α is back stress due to kinematic hardening. σ^{red} is reduced stress.

2.5 Failure and fracture

Failure of a material can be defined as inability of a material to withstand the load beyond certain limit (beyond its load bearing capacity). Failure plays a vital role in

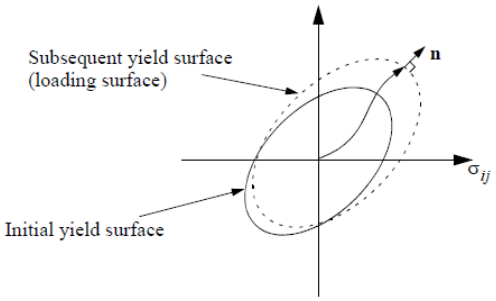

Figure 2.5: Mixed hardening [10]

evaluating the structural integrity of the material. Failure can be broadly classified as microscopic failure and macroscopic failure.
Microscopic failure mainly deals with crack initiation and propagation. Consequently, failure leads to fracture i.e. when the material looses the capacity to bear the applied load, cracks are generated which in-turn finally leads to separation of the material. Failure of material might even be due to material and geometric instabilities. Fracture is defined as material disintegration into two or more fragments under the action of external loads. Fracture can be classified into two types namely ductile fracture and brittle fracture. The phenomenon of fracture mainly depends on the type of material, temperature, state of stress, rate of loading etc. [15].

2.6 Damage Mechanics

Damage mechanics is defined as a study that is concerned with modelling of damage based on initiation, propagation and fracture of the material. Damage mechanics is developed based on continuum damage mechanics. A criterion is needed to predict initiation of damage. A hardening function controls the damage evolution. Characterisation of damage is initiated by nucleation and growth of voids in the material. The instantaneous cross sectional area withstanding the external force progressively decreases until the material separation is initiated, resulting in softening of the material. Damage (D), is the measure of reduced area (due to voids, crack growth, defects) in the material which is seen in the Figure 2.6. Mathematically it is ratio of defective area to the initial area.

$$D = \frac{A_c}{A_{total}} = \frac{A_{total} - A_{reduced}}{A_{total}}$$

When damage tends towards unity, the material will fail as the damage area is same as nominal area. Reduction of cross section has a direct effect in the stress values, thereby stiffness of the material is reduced according to Equation 2.13.

$$\sigma^* = \sigma[1 - D] \tag{2.13}$$

where σ^* = Effective stress
D = Damage

σ = Instantaneous stress

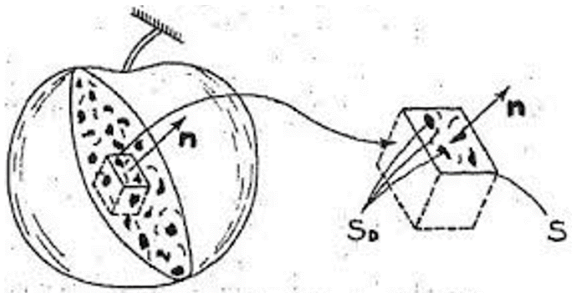

Figure 2.6: Damage Mechanics [9]

2.7 Optimization

Optimisation is defined as the process of identifying the most suitable solution under prescribed conditions by maximising the required objective function and minimising the errors that might exist. Cost effectiveness, efficiency and accuracy are some of the major parameters considered while performing optimisation. Optimisation techniques are also used in stochastic analysis and the solution of system identification problems.

There are many techniques to solve arbitrary nonlinear optimisation tasks. A few of the generally used methods are Successive Response Surface Method, Multidisciplinary optimisation, Sequential with Domain reduction method etc. According to Figures 2.7 and 2.8, optimisation techniques have been broadly carried out in two stages namely: Optimisation process and Optimization results.

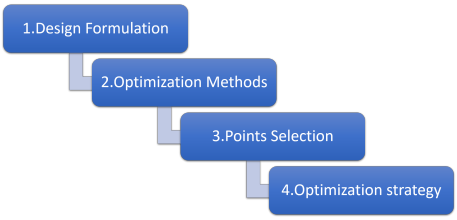

Figure 2.7: Optimisation Process

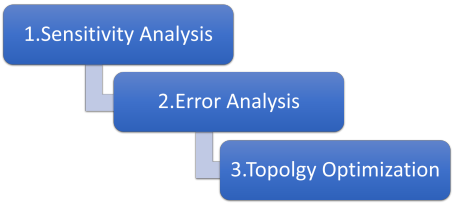

Figure 2.8: Optimisation Results

2.8 Finite Element Modelling

FEM is one of the powerful tools used to find solutions for complex numerical problems for a wide range of engineering problems. This technique mainly deals with analysis of a complex region by defining a continuum subjected to discretisation into simple polygons (triangles, quadrilaterals, hexagons etc) called finite elements. The

material properties and governing equations are applied over these elements and expressed in terms of unknown values. A set of equations are generated by combining all the constraints along with the loads applied. Solutions for set of equations is achieved by various numerical techniques. The solutions obtained predict the approximate behaviour of the systems [14]. Applications of FEM range from stress analysis of a complex system like aircraft, automotive, building, etc to thermal analysis of heat flux, magnetic flux, and other flow problems. There are two main types of elements used in this thesis, shell and solid elements.

1. Solid elements are three dimensional finite elements used to model structures without geometrical simplifications. The use of 3D finite solid elements is proved to be advantageous as it doesn't require geometric, constitutive and loading assumptions. Pragmatic boundary conditions are applied. FE model developed using 3D solid elements replicates the actual CAD model [22]. Solid elements are usually modelled in tetrahedron or hexahedron shapes according to the CAD model. But FE modelling of solid elements makes a design computationally expensive.

2. Shell elements are the simplified formulations of solid elements in a finite element approach to reduce the model and computational time. They are one of the most sophisticated elements as they exhibit both membrane and bending deformations. Shell elements are formulated on the principle of virtual work for 3D continuum models [13].

3

Material Modelling

3.1 Material Models in LS-DYNA

Based on the characteristics of the material, the solver LS-DYNA has categorically classified material models. For example, *MAT_ELASTIC is an isotropic hyperelastic material model which can be used for beams, shells and solid elements. Apart from the predefined models available in solver library, custom material models could also be used. LS-DYNA offers material models based on anisotropic plasticity, cohesive property, concrete property, composites, polymers, orthotropic, viscoelastic, viscoplastic strain rate formulation etc. Hence the user is allowed to select the material model based on the application.

3.1.1 *MAT_ADD_EROSION

Failure and erosion of the elements are not supported by many of the constitutive models in LS-DYNA. Determinination of integrity of the structure is assessed based on material failure. Hence to achieve failure and erosion in complex load cases, LS-DYNA provides an additional supportive material model called "*MAT_ADD_EROSION" which has to be coupled with other constitutive models. The main theory behind the model is to define failure criteria and once the element satisfies the necessary criterion, the element is deleted. This model provides two failure models namely "**G**eneralized **I**ncremental **S**tress-**S**tate dependent damage **MO**del" (**GISSMO**) and **D**amage **I**nitiation and **E**volution **M**odel (**DIEM**) models. These models have options used to define the failure of the material based on different conditions.

3.1.1.1 GISSMO

Generalized **I**ncremental **S**tress-**S**tate dependent damage **MO**del" (**GISSMO**) is a damage model available in LS-DYNA that allows incremental softening and failure, that leads to mapping the process of damage accumulation. GISSMO primely uses a constitutive model to predict the uniform plastic behavior. It is intended to provide possible inputs of a damage definition. An instability curve, failure curve, damage exponent and fading exponent etc. are the necessary parameters to define the GISSMO model

GISSMO is based on an incremental formulation of damage accumulation:

$$\Delta D = \frac{DMGEXP \times D^{(1-(\frac{1}{DMGEXP}))}}{\epsilon_f} \Delta\epsilon_p \tag{3.1}$$

where,

- DMGEXP = Exponent for nonlinear damage accumulation
- D = Damage value
- ϵ_f = Equivalent plastic strain
- $\Delta\epsilon_p$ = Equivalent plastic strain increment

The rate of damage is integrated to obtain a relation between plastic strain and failure strain.

$$D = (\frac{\epsilon_p}{\epsilon_f})^{DMGEXP} \tag{3.2}$$

where ϵ_f = constant

Damage is governed by the Lemaitre equation [8]

$$\sigma^* = \sigma(1 - D) \tag{3.3}$$

DCRIT (function of triaxiality and equivalent plastic strain to failure) and FADEXP (function of triaxiality and instability strain) are the parameters which controls post critical behavior that governs softening and damage accumulation progressively.

$$\Delta F = \frac{n}{\varepsilon(\eta^*)} F^{(1-\frac{1}{n})} \Delta\varepsilon^p \tag{3.4}$$

$$\sigma^* = \sigma[1 - \left(\frac{D - D_{CRIT}}{1 - D_{CRIT}}\right)^{FADEXP}] \tag{3.5}$$

GISSMO allows for calculation of pre-damage for forming and crashworthiness simulations.

Triaxiailty (η) is one of the other important parameters that GISSMO depends on. This triaxiailty is the measure of current stress state and mathematically is the ratio of hydrostatic stresses and von Mises stress. Lode parameter (L) is also an additional measure of current stress state.

$$\eta = \frac{\sigma_H}{\sigma_{VM}}$$

where ,

$$\sigma_H = \frac{\sigma_1 + \sigma_2}{3} \tag{3.6}$$

$$\sigma_{VM} = \sqrt{{\sigma_1}^2 + {\sigma_2}^2 - \sigma_1 * \sigma_2} \tag{3.7}$$

3.1.1.2 DIEM

Damage **I**nitiation and **E**volution **M**odel (**DIEM**) is a damage model which is defined by specifying different damage initiation and evolution criteria. Initiation/Evolution types are defined at each integration point consisting of a damage initiation variable (ω_D^i) and evolution history variable (D^i) such that

$$\omega_D^i \in [0, \infty) D^i \in [0, 1] \tag{3.8}$$

where i=1,2,.....n

Damage evolution governs the damage of the material. Damage initiation might be caused with evolution types as mentioned below:
1. Ductility based on stress triaxiality (Shear initiation, Forming Limit Diagram (FLD) initiation criteria)
2. Ductility based in normalised principal stress

Advancements in CAE industry, has facilitated robust material models that replicate the physical test results effectively and efficiently. Many of the automotive OEMs (**O**riginal **E**quipment **M**anufacturer) found the process of defining material models (using the available information) in virtual environment to be streneous and time consuming. Based on the solver profile and with the coordination of material suppliers and the industry, this requirement was fulfilled by an external distributor.

3.1.2 MATFEM material models

MF GENYld+ CrachFEM [30] is a customised modular material model which is modelled using the constituent modelling options available in LS-DYNA. These material models are provided by an external vendor. MF GENYld+ CrachFEM, is a comprehensive material and failure model that consists of explicit FE codes based on yield criteria and hardening rules [30]. It also summarises different phenomena for material failure. From Figure 3.1, the model uses a modified yield surface which is used to compensate for anisotropic behavior using Equation 3.9.

$$k(\eta) F(\sigma) = \sigma_{eq} \tag{3.9}$$

where,

- k = stress-state dependent correction factor
- $F(\sigma_{ij})$ = symmetrical reference yield locus

CrachFEM consists of three different criteria for localised necking, shear fracture and ductile fracture. It usually considers the equivalent plastic strain (ϵ_{eq}) and failure plastic strain (ϵ_f) to deduce the fracture. Therefore fracture risk (ψ) can be defined as

$$\psi = \frac{\epsilon_{eq}}{\epsilon_f} \tag{3.10}$$

The prediction of localised necking is also included in the CrachFEM algorithm which is usually based on kinematic hardening model. Ductile fracture is computed

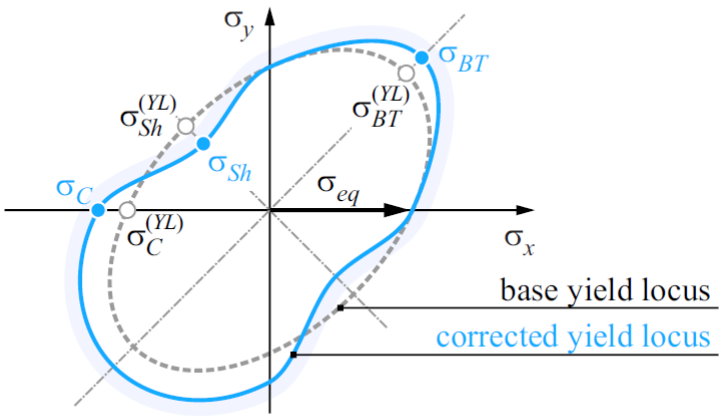

Figure 3.1: Yield locus correction (Image from CrachFEM User's manual) [30]

by considering triaxiality and strain rate while the shear fracture is computed by considering the shear stress parameter and plastic strain rate.

4
Method

The thesis work was broadly classified into two tasks. The first task involved modelling of coupon test specimens with fine meshes of solid elements and validation of those results against the experimental test results. The second task involved conversion of the solid element coupon test models to shell element models (including damage model) also validated against the experimental test results. These results are also compared to results obtained from CrachFEM material models. The schematic work flow is illustrated in the Figure 4.1.

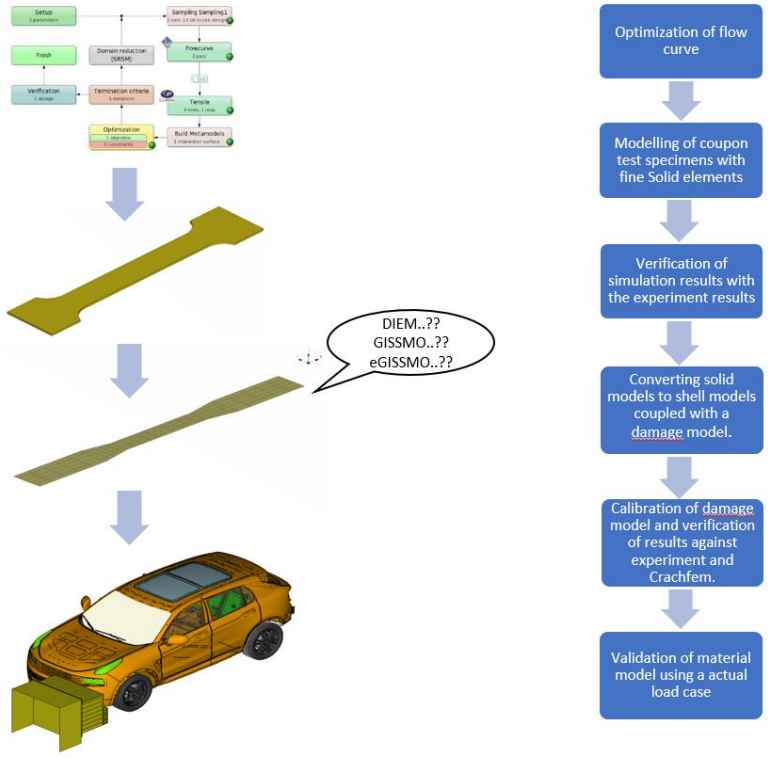

Figure 4.1: Schematic work flow

All FE models were based on the experimental test procedures conducted on DP steel by an external supplier - MATTEST. Nine different experiments were conducted by the supplier to characterise the material. The detailed description of the specimens and test procedures are discussed below. The tests fall under two categories, tests to describe plastic behavior and tests that describe fracture.

List of Experiments:

- Uniaxial tension
- Torsion
- Layered Compression
- Tension of specimen with groove
- Tension of specimen with hole
- Unibiaxial test
- Shear test
- Bend test

4.1 Tests to describe plastic properties

Uniaxial tensile tests

Quasi static (nominal strain rate 0.001/s) and elevated strain rate uniaxial tensile tests were conducted with loads applied 0, 45 and 90 degrees to the rolling direction. The 0.2% yield strength, strain hardening and plastic anisotropy 'r' (Lankford coefficient) were derived from these tests for each orientation. The uniaxial tensile tests were also used to derive limit strain for localized necking.

Figure 4.2: Schematic representation of Uniaxial tension test [30]

Layered compression test

The layered compression test was conducted using a stack of round discs subjected to uniaxial compression in the direction of sheet thickness. Strain hardening for higher strain rates were measured in this test.

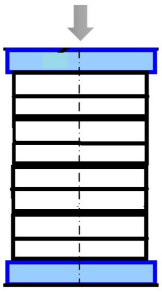

Figure 4.3: Schematic representation of Layered compression test [30]

In-plane torsion test

Yield strength in pure tension could be determined using this test. The circular specimen with a circular groove was used in this test. Groove dimensions were decided such that the deformation was concentrated in the groove during loading. The tension diagram was obtained as angle ϕ over torque M_i.

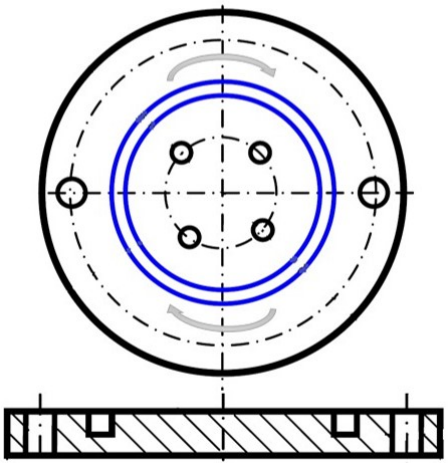

Figure 4.4: Schematic representation of In-plane torsion test [30]

4.2 Tests to describe fracture properties

The following tests were performed to determine the limit curves for ductile normal fracture and ductile shear fracture.

Biaxial test or Erichsen test

This test was performed to determine the equivalent plastic strain at fracture for equibiaxial strain. Minimum sheet thickness at the crack was measured.

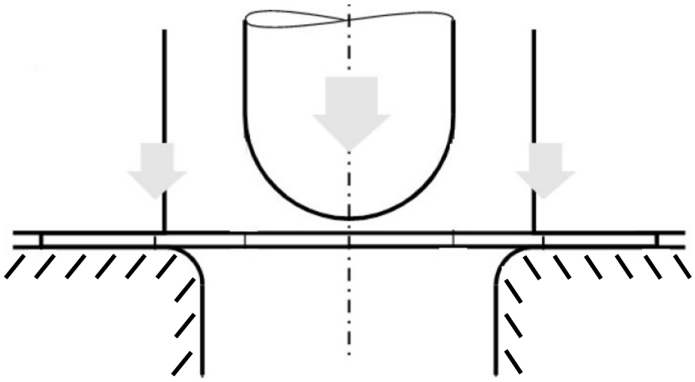

Figure 4.5: Schematic representation of Uni-biaxial test [30]

Three-point bending test

Rectangular specimens with longer edge aligned with the rolling direction were used in this test. Plane strain condition was assumed during bending by keeping the width of the specimen five times greater than the thickness. The maximum possible strain upto the fracture was determined from the maximum curvature.

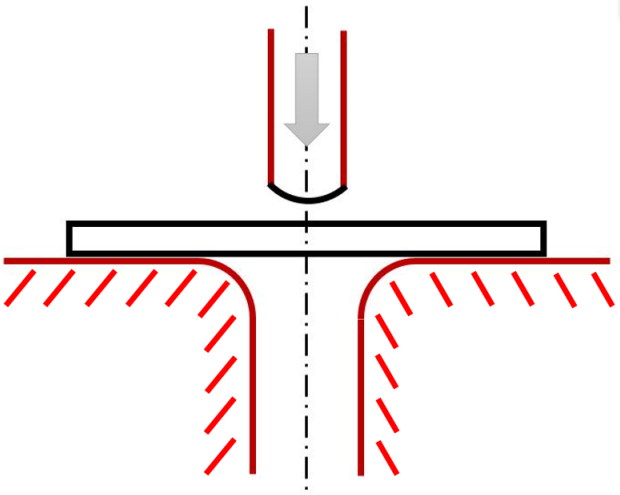

Figure 4.6: Schematic representation of Three point bending test [30]

Tensile test of a thin strip with hole

A thin metal specimen with a hole (with the diameter half the specimen's width) was subjected to load in the longitudinal direction until fracture. The longitudinal direction and rolling direction of the specimen were aligned and ductile normal fracture was observed in the specimen at failure. Equivalent fracture strain was determined at the rim of the hole. The thinning of the hole at the rim and the anisotropy value was calculated in load direction.

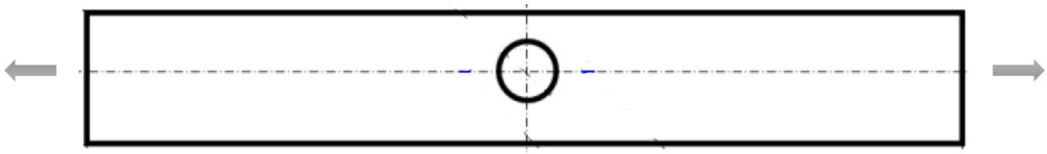

Figure 4.7: Schematic representation of Tension test (specimen with a hole) [30]

Tensile test for specimen with waist

This is an alternative tension test for the determination of the equivalent plastic strain at fracture for the condition of plane strain. The specimen with waist was optimised to cause localised necking at the centre of the specimen. The fracture strain is derived from the thinning of the fractured part at the specimen centre.

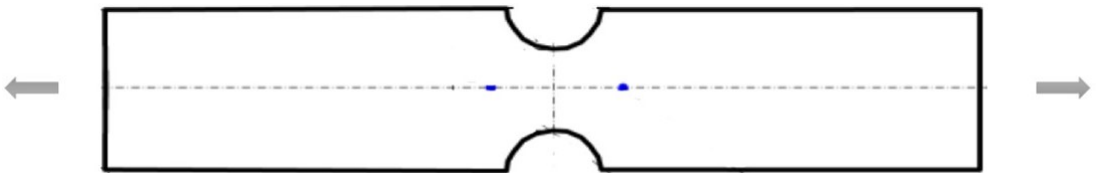

Figure 4.8: Schematic representation of Tension test (specimen with a waist) [30]

Tensile test with a groove

A specimen with groove was subjected to tensile test. In the specimen, the groove was oriented by 90 degrees to the loading direction (to achieve plane strain condition in the groove). The equivalent plastic strain at fracture was determined from the final sheet metal thickness. Shear fracture was observed in the specimen.

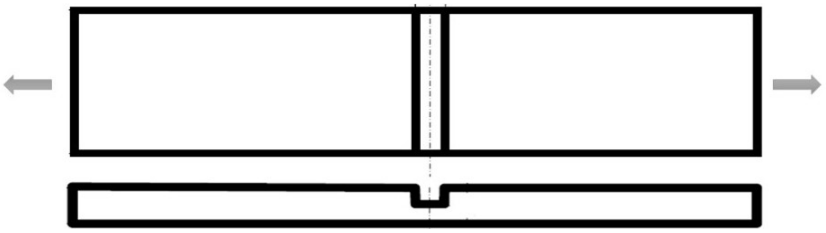

Figure 4.9: Schematic representation of Tension test (specimen with a groove) [30]

Shear test

Since the torsion test was prone to instability inside the circular groove before fracture, another test was performed to determine the effective plastic strain at fracture under pure shear. This rectangular specimen with two parallel grooves was loaded in-plane at the centre of the specimen which causes shear deformation in the groove. *Note: Exact experimental setup and boundary conditions were unknown.*

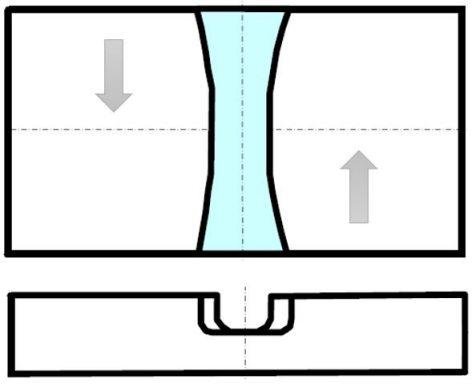

Figure 4.10: Schematic representation of In-plane shear test [30]

Virtual laboratory - Finite Element models

FE models developed for the current study are presented in the Figure 4.11.

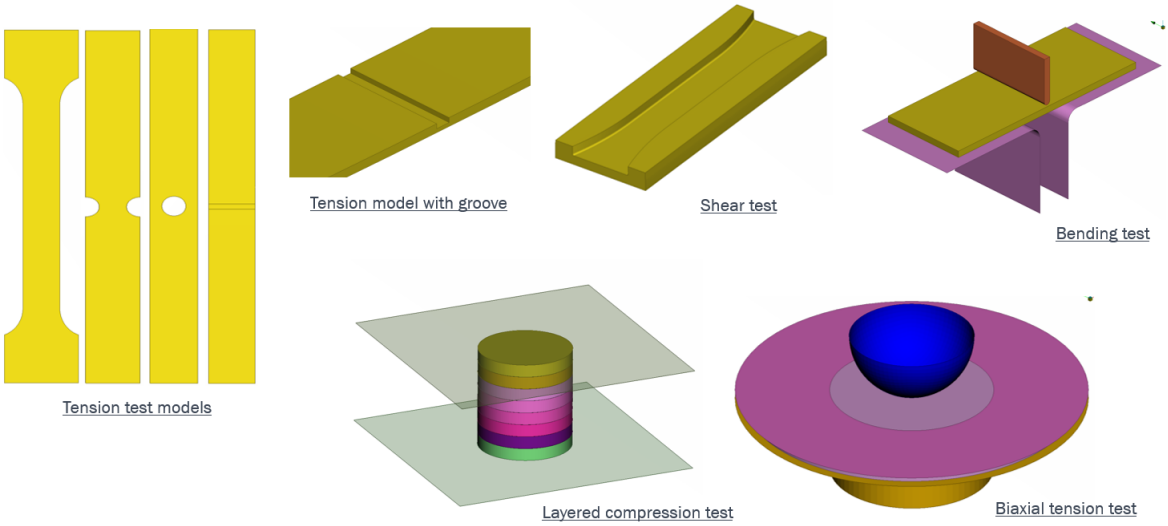

Figure 4.11: FE test specimens

4.2.1 Optimization of Hardening curve

After the modelling of test specimens, a hardening curve for the simulation was selected by extrapolating the true stress-strain curve. Different hardening rules were used to extrapolate the true stress-strain curve(obtained from the experimental test data) as shown in the Figure 4.12. Here strictly increasing slope condition was considered, in order to avoid negative slope in the hardening curve.

Figure 4.12: Flow curves extrapolated from different hardening rules

From Figure 4.13, it was observed that the initial elastic region and plastic region until the ultimate strength limit might not match with the experimental test results. Hence in the current study, this method was found to be not feasible to proceed in the development of virtual test lab. Another approach to overcome this problem, was to consider the true stress-strain curve (from the experimental test result) until the ultimate strength point and extrapolating it using different hardening rules. By this method, experimental results could be matched exactly up to the ultimate strength limit.

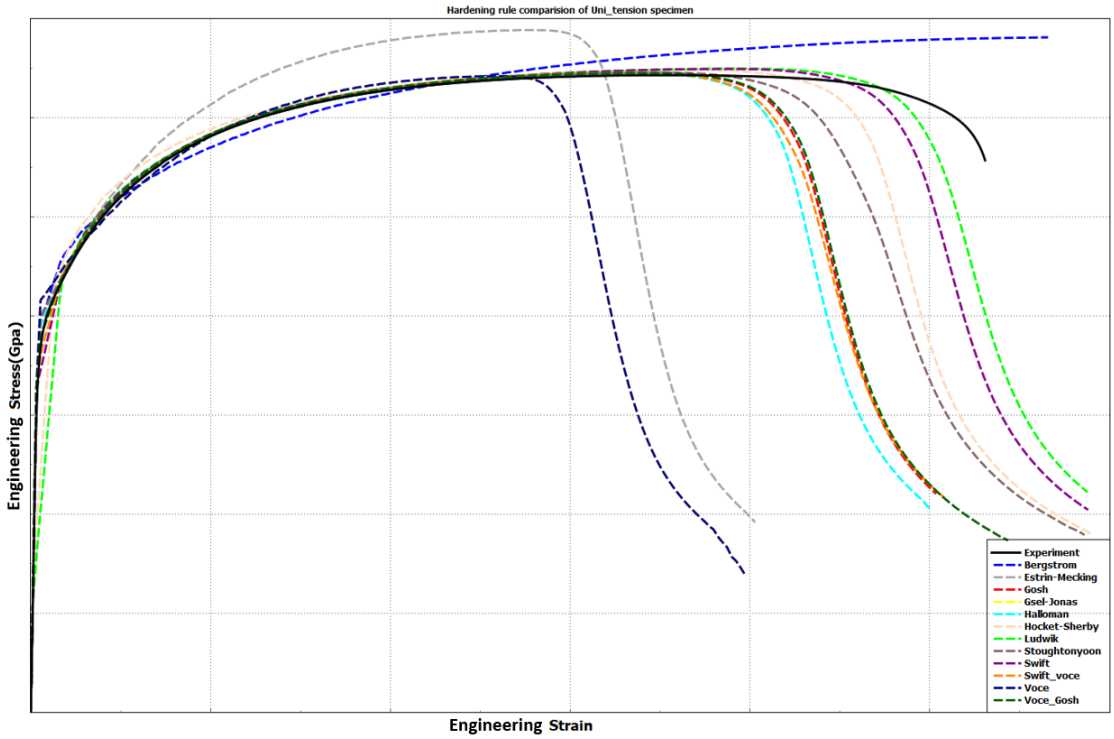

Figure 4.13: Engineering stress-strain plot from different hardening rules

A new methodology has been implemented with the help of an optimiser and same is explained in the following section. A meta model-based optimization setup in LS-OPT is shown in Figure 4.14. The two stage optimization process is explained below.

1. **Setup** : In the global problem setup stage, the end points of the true stress-strain curve at the ultimate strength i.e stress and stain values defined as parameters in the ".key" file were automatically detected. These parameters were then defined as a continuous variables with lower and upper boundaries assigned to the initial value.
2. **Sampling** : Different metamodel settings were defined in this stage. A polynomial, quadratic order Successive Response Surface Method (SRSM) was used in the optimization study with Latin Hypercube point selection for sampling.
3. **Flowcurve** : User defined python script computes and extrapolates the input true stress-strain curve from the experiment using the parameters defined in the setup stage and the extrapolated flow curves in each iteration were copied to the respective iteration folders in the 'Tensile' stage for the main simulation.

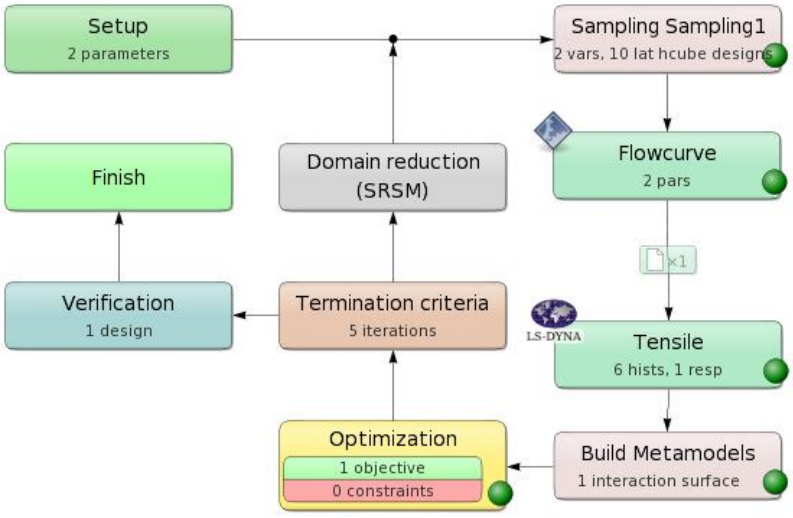

Figure 4.14: Optimization setup

The program extrapolates the curve with strictly increasing slope condition to avoid negative slope in the flow curve.

4. **Tensile** : The flow curve from the previous stage was used as an input curve to the material model *MAT_24 and simulation of uniaxial tensile test was performed. Time histories like nodal output (NODOUT) and section forces (SECFORC) were defined to plot the stress-strain curve from the simulation. A curve matching objective was defined as a composite in this stage. This composite matches the history with the response and combines the response surface into a single expression.
5. **Optimization** : After the simulation, the metamodel, which is nothing but an approximation to the design response, starts to build according to the metamodel setting. An optimization process starts with a partial curve mapping algorithm to match the simulation curve with experimental curve as per the objective defined in the previous stage.
6. **Domain reduction** : After each iteration, SRSM reduces the domain with all points within a sub-region. It moves the region of interest towards the optimal solution within the design space by ignoring the points belonging to the previous iterations. If the approximated solution converged, SRSM writes the final solution. If not, the loop continues with the reduction of domain towards the optimum until it meets the termination criteria.
7. **Termination** : Each design terminates after a specific number of iterations specified in this stage along with the tolerance between the design, objective and metamodel accuracy.

The schematic representation of optimization process is shown in Figure 4.15. Simulation history, optimization history and the metamodel response surface was plotted in the post processing. Based on the results obtained from the optimization process, suitable design and corresponding input flow curve was selected. From Figures 4.16 and 4.17, the simulation history and the metamodel response surface can be viewed.

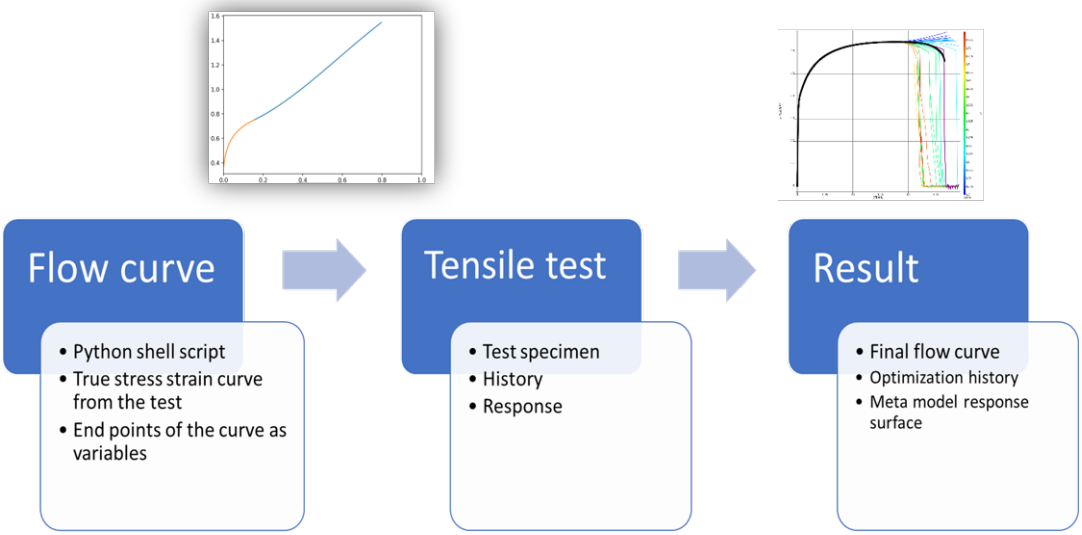

Figure 4.15: Optimization work flow

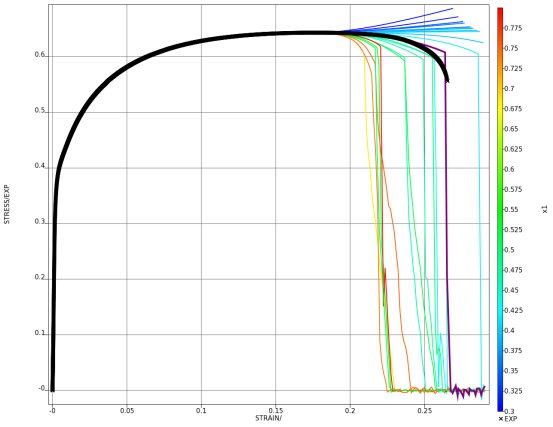

Figure 4.16: Optimisation Result

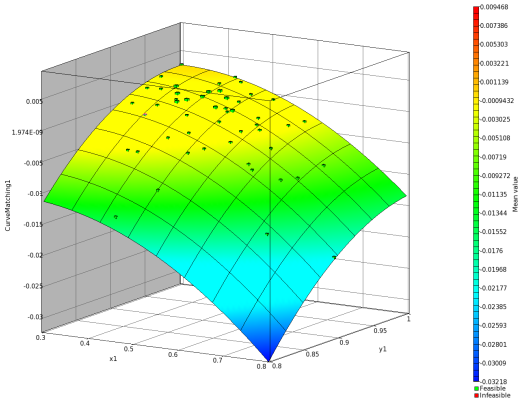

Figure 4.17: Response surface

4.2.2 Solid element models

All test specimens were developed using a fully integrated solid elements of element formulation '-1' (ELFORM= -1) which takes care of elements with poor aspect ratio. Fine element (<0.2mm) meshes were used at the critical region to capture the deformation behaviour as shown in Figure 4.18. From Figure 4.19, it is visible that grooves in the tension and shear specimen were modelled with fine element meshes involving many layers in the groove thickness. This type of modelling helps capture the instability effectively. The accuracy of solid element models was verified against the theoretical triaxiality values. The effective plastic strain was considered as failure criteria in all solid element models.

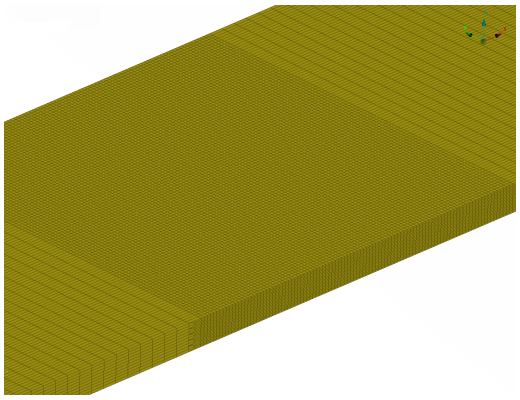

Figure 4.18: Tension test model

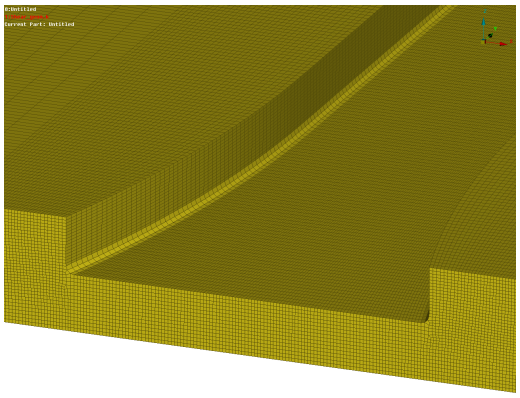

Figure 4.19: Groove in shear model

4.2.3 Shell element models

Shell element models were developed from the solid element models after they were calibrated against the experimental results. All shell element models were modelled with a fully integrated shell elements (ELFORM=16) and five integration points across the thickness (NIP=5). Figures 4.21 and 4.22 shows the elements in the groove region pertaining to tension and shear specimen were represented with the exact thickness offset. This type of modelling was carried out to mimic the exact groove geometry.

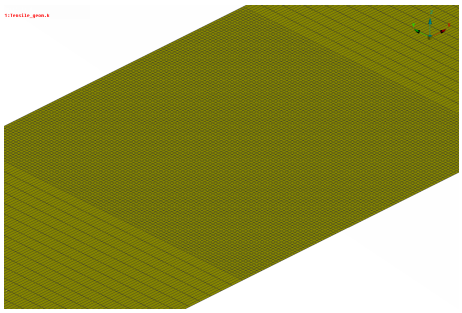

Figure 4.20: Shell tension model

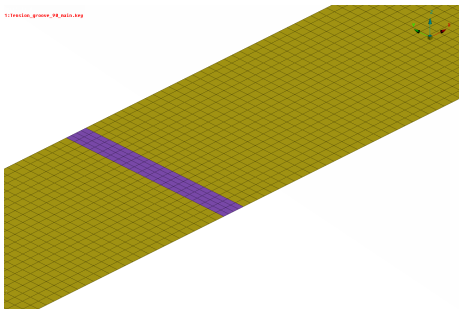

Figure 4.21: Groove in shell model

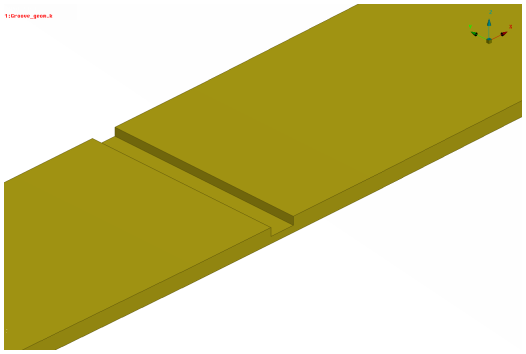

Figure 4.22: Thickness offset in the groove

4.2.4 Material model

An elasto-plastic isotropic material called *MAT_PIECEWISE_LINEAR_PLASTICITY (*MAT_24) was used to characterise the material for both solid and shell models. A typical material card in LS-DYNA is shown in the Figure 4.23. The fracture model was defined using an auxiliary model called *MAT_ADD_EROSION in LS-DYNA. Important input parameters in *MAT_24 card are,

- MID : Material ID
- RO : Material Density
- E : Elastic modulus
- PR : Poisson's ratio
- LCSS : Stress-strain curve (Flow curve)

```
*KEYWORD
*TITLE
*MAT_PIECEWISE_LINEAR_PLASTICITY_TITLE
Default MAT24 MAT_PIECEWISE_LINEAR_PLASTICITY
$#     mid        ro         e        pr      sigy      etan      fail      tdel
    100000  7.850E-6     210.0       0.3     0.352       0.0       0.0       0.0
$#       c         p      lcss      lcsr        vp
       0.0       0.0         1         0       0.0
$#    eps1      eps2      eps3      eps4      eps5      eps6      eps7      eps8
       0.0       0.0       0.0       0.0       0.0       0.0       0.0       0.0
$#     es1       es2       es3       es4       es5       es6       es7       es8
       0.0       0.0       0.0       0.0       0.0       0.0       0.0       0.0
*MAT_ADD_EROSION
$#     mid      excl    mxpres     mneps    effeps    voleps    numfip       ncs
    100000       0.0       0.0       0.0       0.0       0.0       1.0       1.0
$#  mnpres     sigp1     sigvm     mxeps     epssh     sigth   impulse    failtm
       0.0       0.0       0.0       0.0       0.0       0.0       0.0       0.0
$#    idam    dmgtyp     lcsdg     ecrit    dmgexp     dcrit    fadexp    lcregd
          1       1.0         7        -8         8       0.0    8.3452         9
$#  sizflg     refsz     nahsv     lcsrs    regshr    rgbiax
          0      0.50       0.0         0       1.0       1.0
$#   lcfld              epsthin    engcrt    radcrt
          0         0       0.0       0.0       0.0
```

Figure 4.23: MAT_24 material card

Different failure options and damage models could be defined through *MAT_ADD_EROSION model. Some of the important parameters to define and calibrate damage model have been given:

- **MID** : Material ID
- **IDAM** : Flag for damage model
- **DMGTYP** : Damage coupling to stress
- **LCSDG** : Load curve defines equivalent plastic strain to failure vs. triaxiality
- **ECRIT** : Critical plastic strain
- **DMGEXP** : Exponent for non linear damage accumulation
- **FADEXP** : Exponent for damage related stress fadeout
- **LCREDG**: Load curve ID defining element size dependent regularization factors for equivalent plastic strain to failure

The MID of *MAT_ADD_EROSION should be same as the MID of *MAT_24 in order to link the damage model to the constitutive model. The GISSMO damage model was initialised by switching the flag IDAM to 1.

4.2.5 Calibration of GISSMO card

The main parameters to calibrate the GISSMO damage card model are DMGTYP, LCSDG, ECRIT, DMGEXP, FADEXP and LCREDG. The parameter DMGTYP couples the damage to flow stress so that the damage gets accumulated as the material deforms and elements fail when the damage parameter, D=1. This can be activated by switching DMGTYP to 1 in *MAT_ADD_EROSION card.

LCSDG and ECRIT are the key parameters which define the failure in the material based on the triaxiality and instability, respectively. Failure based on the triaxiality can be defined through a load curve for LCSDG. This load curve covers the triaxiality range from -2/3 to 2/3 for the shell elements. The triaxiality values were taken from each solid test at the time of failure and plotted against the equivalent plastic strain at failure. The curve was fitted using spline function.

Instability in the material can be defined through critical strain against triaxiality curve for ECRIT. Critical strain was measured when the force reaches maximum value in the solid test specimens. The critical strain from each test was plotted against the triaxiality of respective load cases. Both the failure and instability curves are shown in Figures 4.24 and 4.25 respectively.

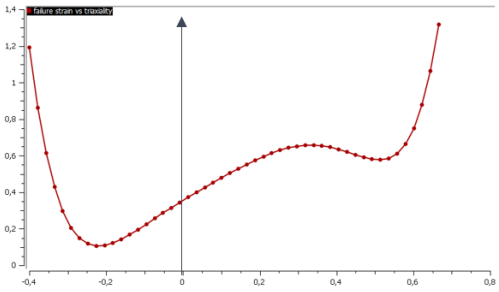

Figure 4.24: Failure strain vs triaxiality

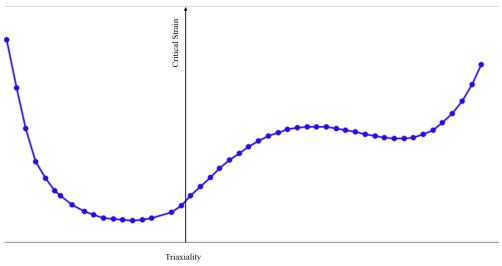

Figure 4.25: Critical strain vs triaxiality

4.2.5.1 Parameter identification: Damage and Fade exponent

DMGEXP and FADEXP plays a decisive role in damage accumulation and stress fading exponent, respectively. According to equation 3.2, DMGEXP allows accumulation of damage in the material. The fading exponent, FADEXP is similar to damage where the instability measure is incrementally accumulated as a function of critical strain based on Equation 3.4. Coupling between stress and damage starts when the instability measure, F=1. As soon as the instability measure F reaches unity, the current damage value D in the elements is stored. These damage values would be helpful in calculating the stress tensor in accordance with Equation 3.5. Thus, continuous reduction of stress occurs until failure i.e when damage measure D reaches unity.

The combination of DMGEXP, FADEXP and EPSF plays a significant role in the overall behaviour of a damage model in predicting the fracture in different stress states. The optimisation technique with LS-OPT was used to understand the influence of these parameters on each other. Sensitivity of parameters was measured by defining each parameter as a variable having the other two as constants.

4.2.5.2 Mesh Regularization

Beyond the point of uniform expansion, the solution is not unique and dependent on the element size. In order to get the damage model independent of element size, fracture strain must be scaled by a scale factor. The scale factor was determined by an optimization of a tension test specimen modelled with a larger element size. The element size against scale factor scaling curve was defined for LCREGD to regularize the mesh size. The result of mesh regularization is discussed in the result section.

5
Results and Discussion

The optimization technique was used to extrapolate the hardening curve (used in the simulations), to predict the failure in the material and the optimal design (hardening curve) from the uniaxial tension test was used to carry out all other load cases. The solid FE models developed in this study have exhibited good correlation with the experimental test results results and predicted the different stress states close proximity to the theoretical triaxiality.

All the necessary information like the triaxiality, failure strain and critical strain was extracted from the solid FE models and the optimization was extensively carried out to identify the parameters DMGEXP and FADEXP to calibrate the GISSMO damage model. Three good designs (set of parameters) were selected from the optimization which resulted in satisfying results in the uniaxial tension test. The three set of parameters are included in Table 5.1.

	DMGEXP	**FADEXP**	**EPSF**
Set 1	6.05178	1.15	1
Set 2	8	8.3452	1
Set 3	3.87211	3.8493	0.84792

Table 5.1: Optimized set of parameters

The tension tests with different element sizes ranging from 0.5mm to 5mm were executed for mesh regularization and the failure strain was scaled across the element size range. Figure 5.1 is the scaling curve for mesh regularization and Figure 5.2 shows the interaction of the post critical region to element size.

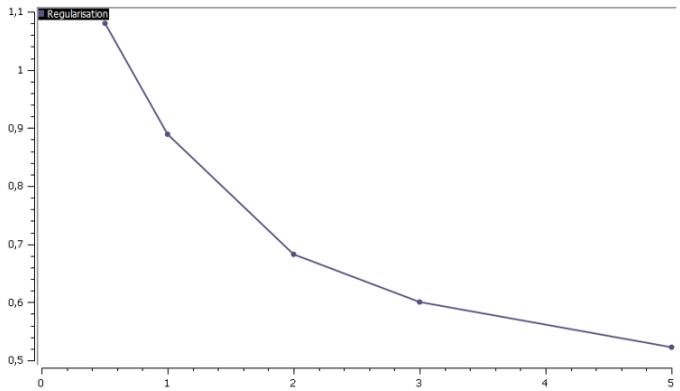

Figure 5.1: Scaling curve

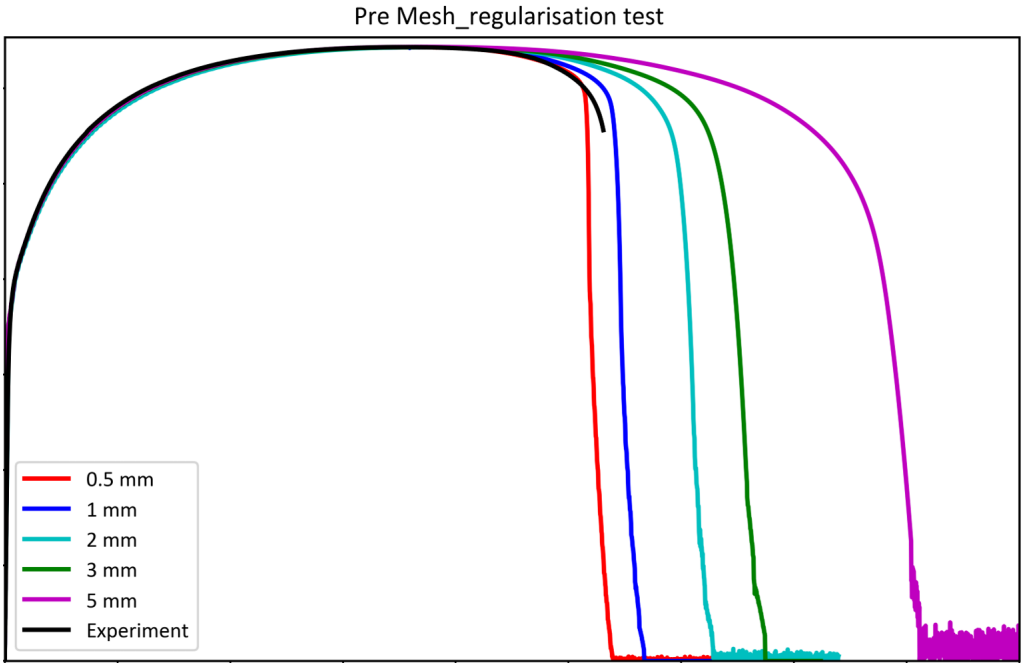

Figure 5.2: Pre Mesh regularization

Figure 5.3 shows the variation of fracture stain is scaled for different element sizes so that result is identical for all element size between 0.5mm to 5mm. Figure 5.4 shows the von Mises stress fringe plot at the time of necking for different element sizes. The calibrated material model was used in all load cases and the results are presented in the following section.

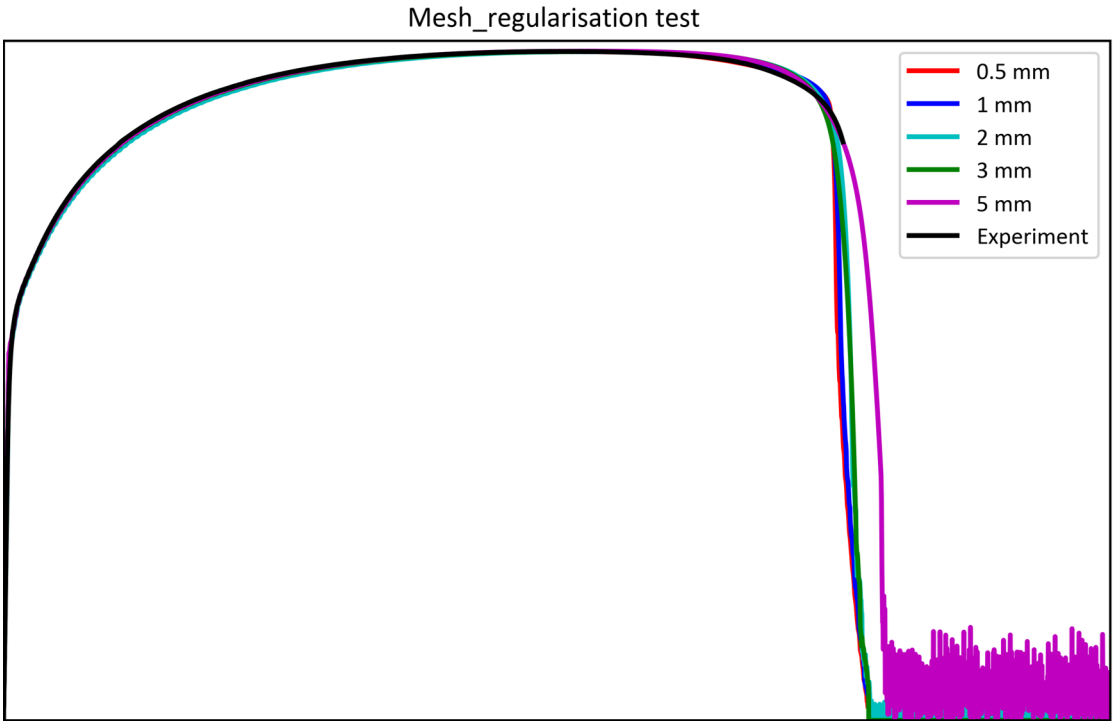

Figure 5.3: Post Mesh regularization

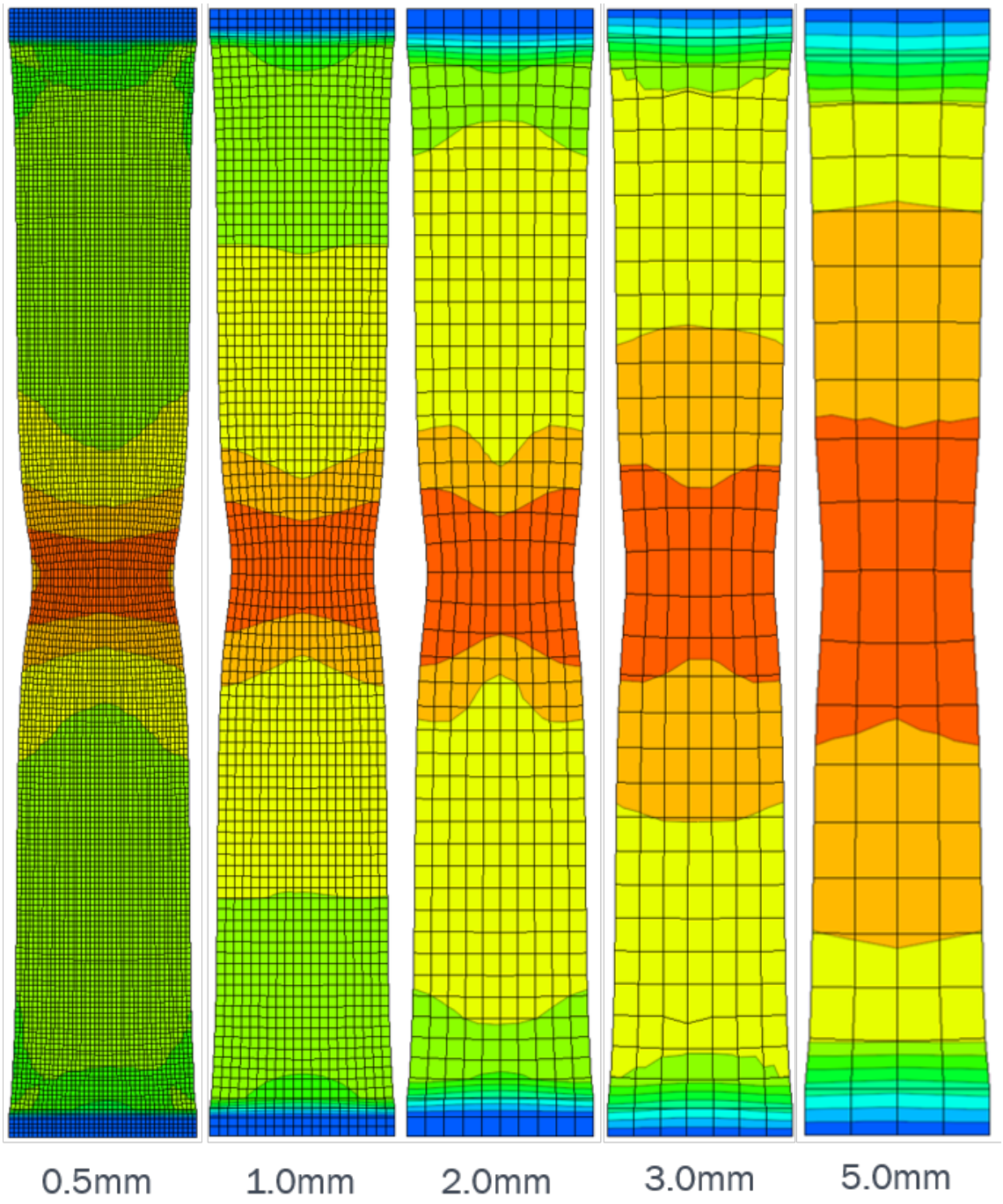

Figure 5.4: Mesh regularization for different mesh sizes

Eight tests were conducted virtually on DP steels and the results are presented in the current section. The plots mainly include experimental test results, solid model results (using *MAT_24) and shell model results (using CrachFEM and *MAT_24+GISSMO). Specially, the uniaxial tension test plot in Figure 5.5, comprises shell model results from all 3 sets of values in Table 5.1, out of which the second set showed promising results not only in tension but in other tests as well. Hence, only the Set 2 results of shell element models have been presented in rest of the plots.

5.1 Coupon test results

The solid models in all tension tests performed, capture the behaviour quite well until the point of uniform expansion. A deviation was observed in the post critical region, as the constitutive model (*MAT_24) alone was uanble to capture the material behaviour. On the other hand, the shell model coupled with damage model captures the material failure quite effectively by calculating the progressive damage in the material. The Set3 from Table 5.1 of the shell models in the uniaxial tension test shown in Figure 5.5 accumulates more damage than Set1. Though Set 1 has high DMGEXP (damage exponent), the lower FADEXP (fading stress exponent) value resulted in less accumulation of damage as the instantaneous stress and FADEXP are exponentially related, (equation (3.5)). The Set2 with approximately equal DMGEXP and FADEXP values showed good correlation with experiments in uniaxial tension test, tension test of specimen with waist and tension test of specimen with hole (Figures 5.5, 5.6 and 5.7) respectively.

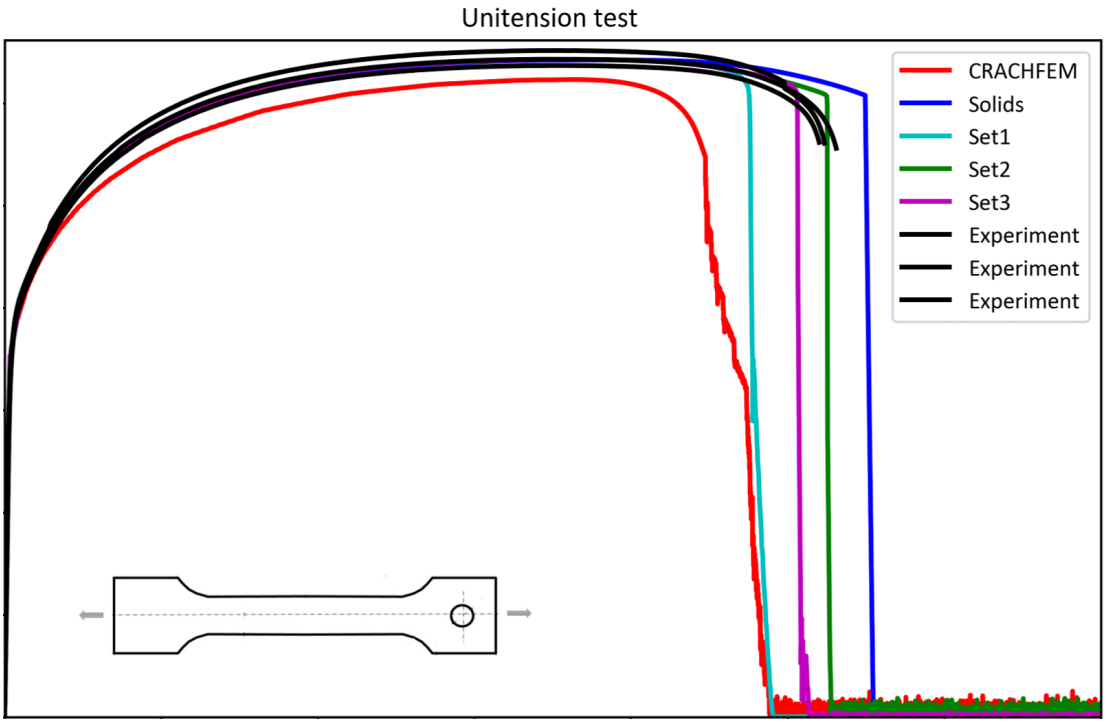

Figure 5.5: Stress-strain curve of an Uniaxial tension test

Both solid and shell models overestimated the force level in the tension test of a specimen with a groove. This was due to the instability in the groove and lack of information about the physical test procedure. On the contrary, it can be observed in Figure 5.8, the results from the CrachFEM material model effectively captured the material failure in the specimen with groove. The same CrachFEM material model in other tension tests showed early softening.

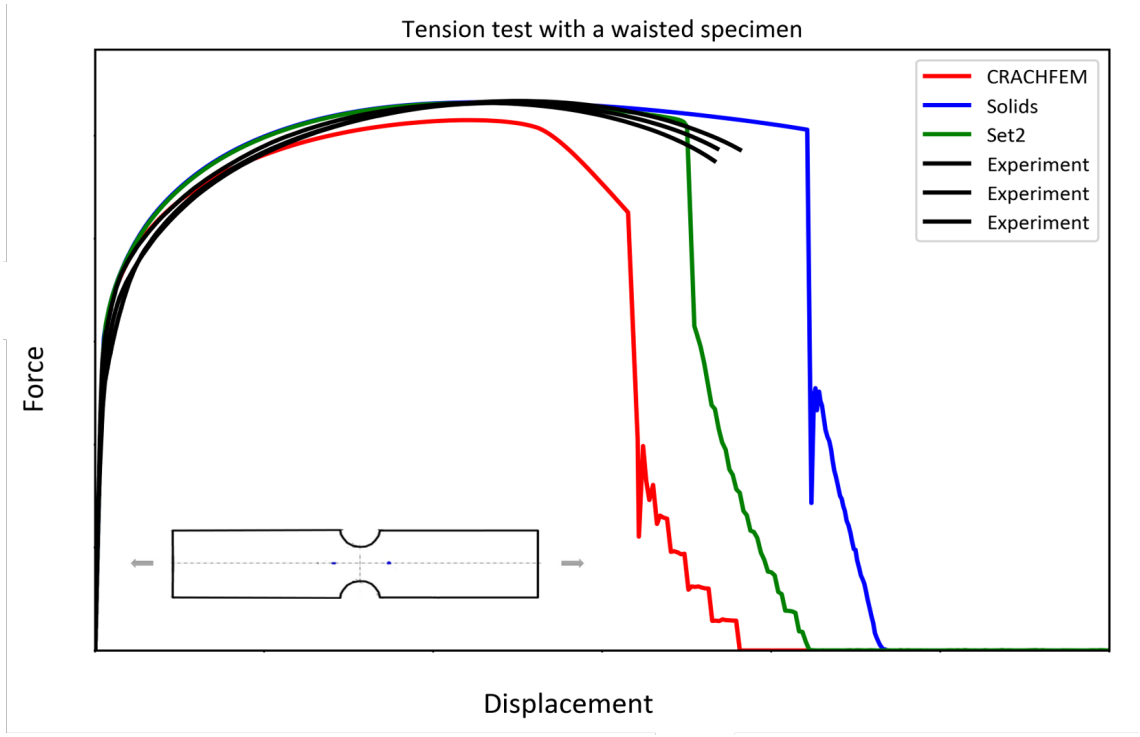

Figure 5.6: Tension test (specimen with a waist)

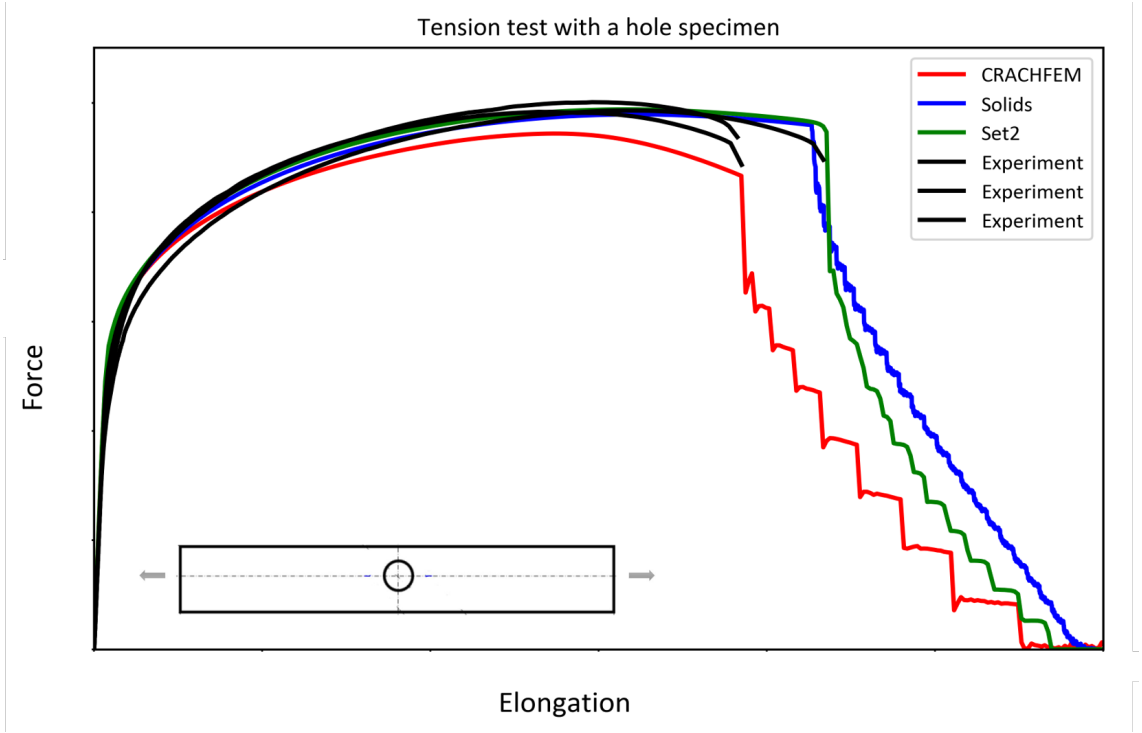

Figure 5.7: Tension test (specimen with a hole)

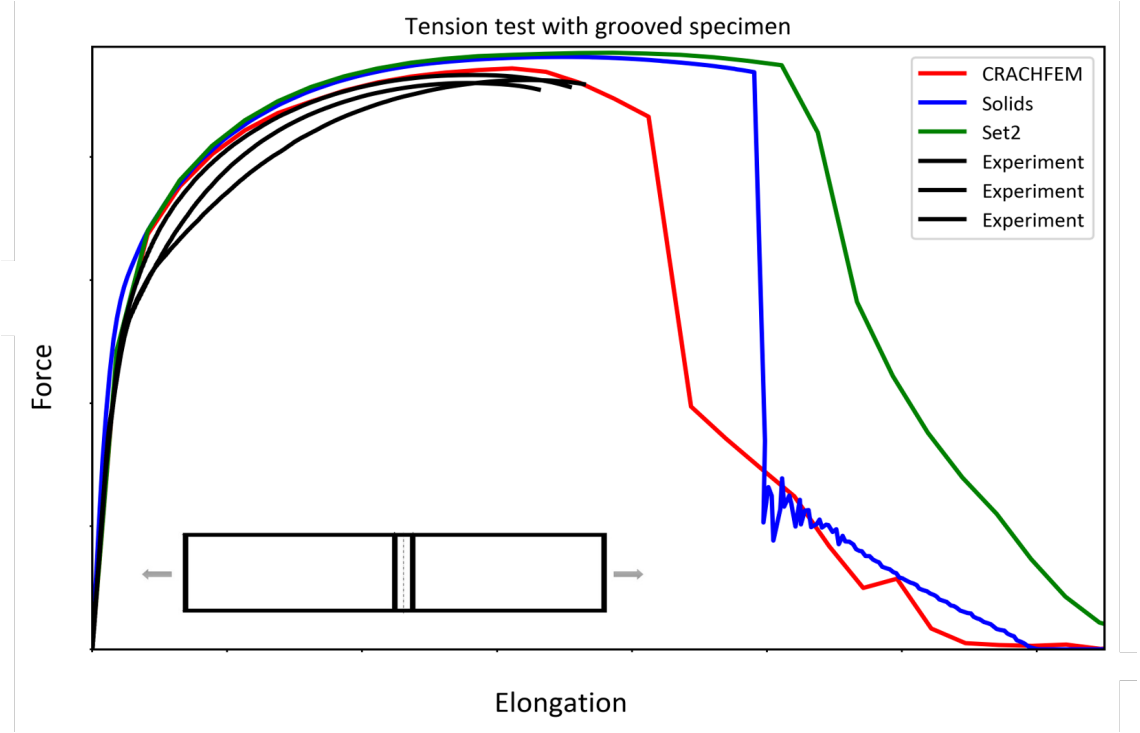

Figure 5.8: Tension test (specimen with a 90° groove)

The solid and shell models are in good agreement with the experiments in three-point bending test. However, both models demonstrated slightly stiff behavior. This is due to the variation of physical test (consisting of roller supports) compared to the numerical test (consisting of fixed supports). Also the friction values used in the experimental test were unknown. CrachFEM, on the other hand, was found to underestimate the force levels.

The Figure 5.10 shows the results obtained for the biaxial stress state in the Erichsen test where the solid element and shell element models (through simulations), match well with the experimental test result. The solid model revealed a crack quite later, when compared to the experiment in the biaxial test or Erichsen test. The shell model was in concurrence with the experimental test result by predicting the crack at the right displacement of the punch. The simulation involving CrachFEM material model, depicted an early failure in the test.

Figure 5.11 shows the correlated results for the layered disc compression test. The test was conducted using solid elements to calculate the material hardening behavior at higher strains. The discs were compressed close to half of its initial height and the increase in the discs diameter was measured and was found to be in accordance with the experimental test result. The shear model with a butterfly notch illustrated right deformation behaviour despite an early failure. The force levels were also underestimated when compared to the experimental test result. Lack of information about the experimental test procedure might be the reason for inaccurate results in the shear test simulation.

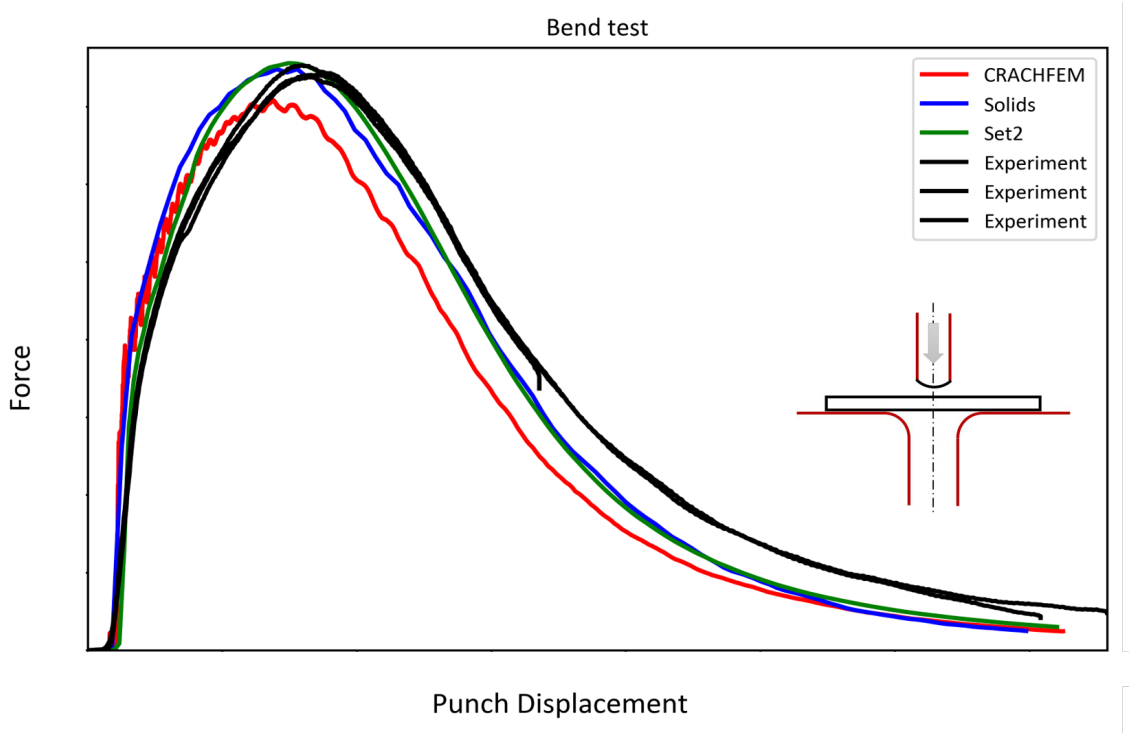

Figure 5.9: Bend test

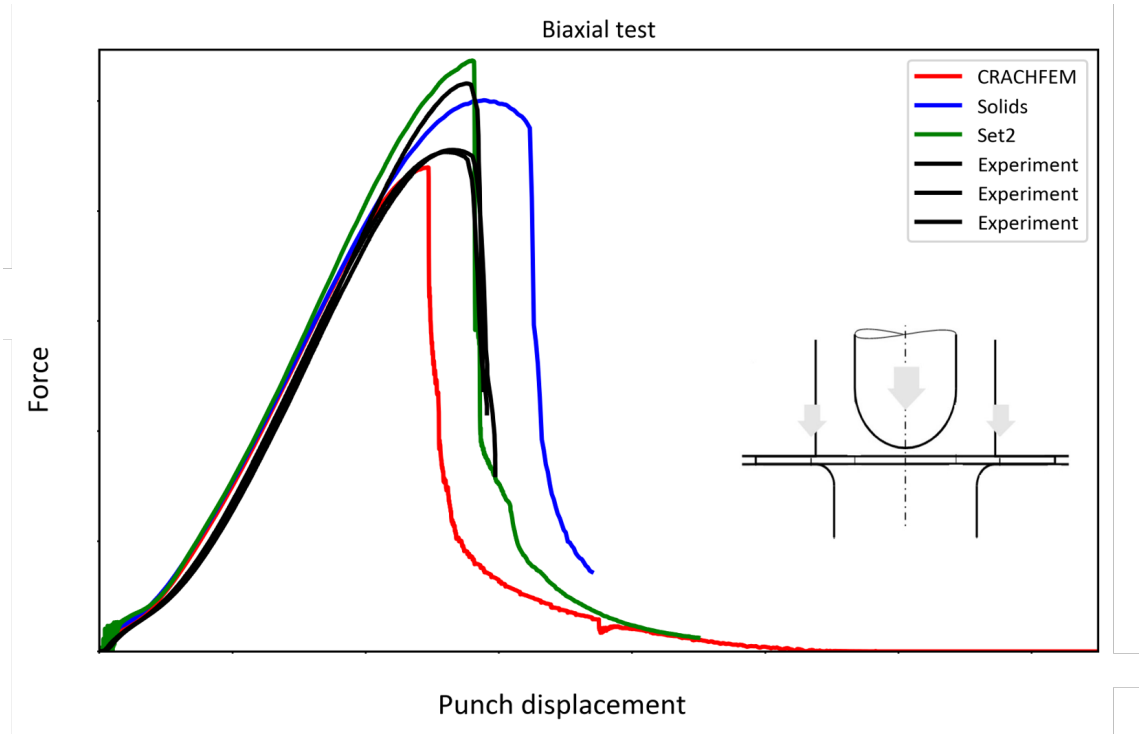

Figure 5.10: Unibiaxial test

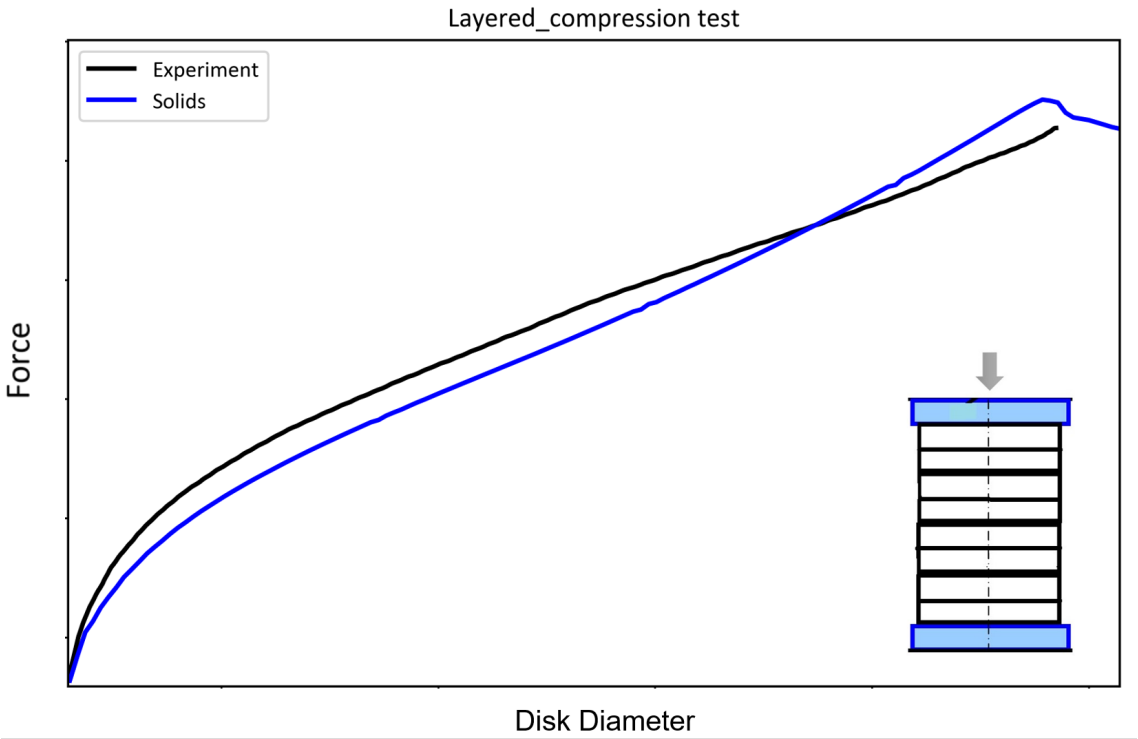

Figure 5.11: Layered Compression test

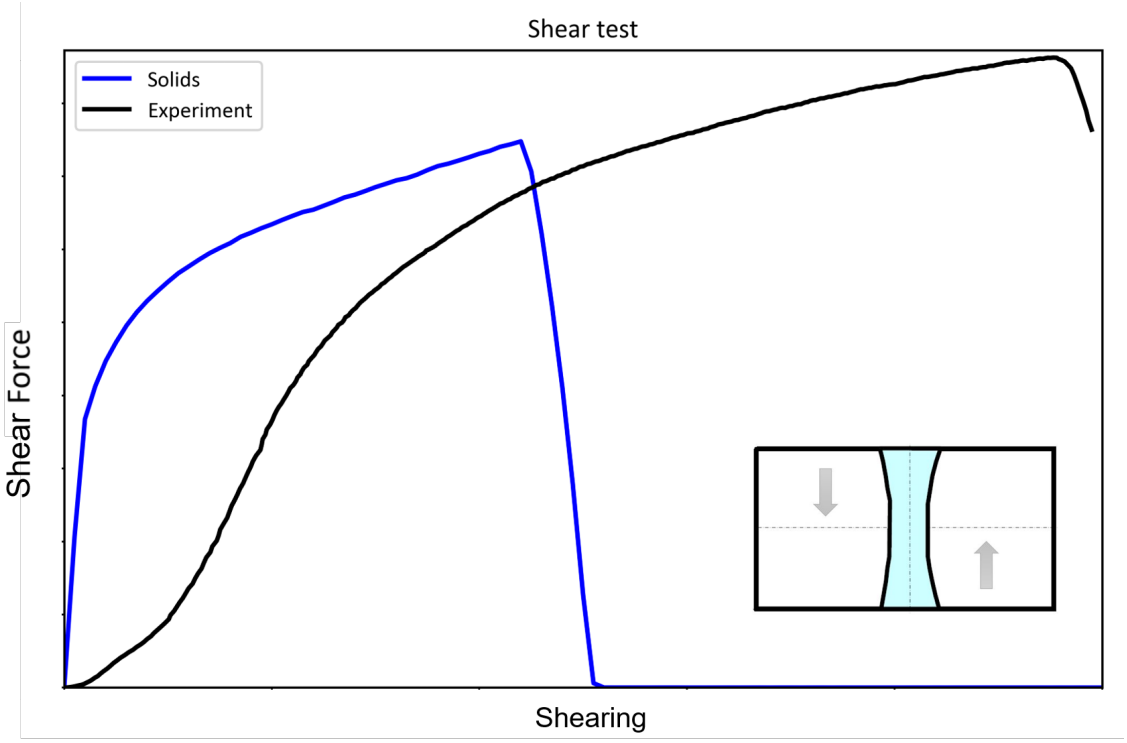

Figure 5.12: Shear test

A significant increase in the computational efficiency was observed in the GISSMO models. The computational time for different load cases between the two models are presented in the Table 5.2.

Tests	CrachFEM	MAT24+GISSMO
Uniaxial Tension test	471s	228s
Tension test (specimen with waist)	468s	313s
Tension test (specimen with hole)	477s	343s
Tension test (specimen with 90° groove)	527s	472s
Bend test	6223s	3329s
Unibiaxial f-erichsen test	2446s	1739s

Table 5.2: Time Comparison table

The dimensions of the cracks after the failure of solid specimens were measured in all load cases and were compared against the dimensions of cracks measured from the physical tests. Overall, a 95% accuracy was achieved with the solid element specimens in comparison with physical tests. The width and thickness at the crack centre was measured in all tension test models. The ductile shear fracture was observed in all tension tests.

The shear test demonstrated good qualitative behavior in comparison with the experiment but the quantitative results failed to do so (due to early failure). This is due to the fact that the complete information on the physical test was unknown. The bending test (involving both tension and compression stress states) exhibits no fracture in the simulation similar to the physical test. Deformation behaviour of unibiaxial test specimen exhibited good correlation with experimental test result but with a crack initiation slightly later in the simulation.

A sheet with a grid was used on the test specimens in bending and unibiaxial tests to measure the strain in the experiments. The same grid dimensions were represented in the simulations using null shell elements which can be viewed in the Figure 5.13. The grids were also used to understand the crack initiation distance from the locus. Crack dimensions of all specimens have been presented in the Table 5.3.

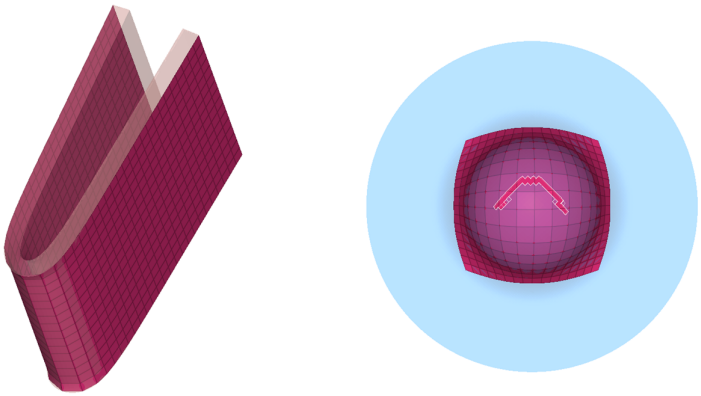

Figure 5.13: Grid Dimensions

		Solid Model	Experiment
Tension test	Width after failure	15.10	16.43
	Thickness at the crack center	0.704	0.622
Tension test grooved specimen	Width after failure	18.79	19.093
	Thickness at the crack center	0.359	0.336
Tension test with a hole	Thickness at the crack center	1.014	0.6793
Tension test with waist	Thickness at the crack center	0.858	0.722
Bending Test	$d_0 Initial$	0.991	1
	$d_0 Final$	1.642	1.56
	$d_{90} Initial$	1.237	1.260
	$d_{90} Final$	1.238	1.256
Compression test	Change in disc diameter	2.4208	2.3778
Shear test	Equivalent strain at fracture**	0.3265	0.8213
Unibiaxial test	$d_0 Initial$	1.655	1.645
	$d_0 Final$	3.148	2.790
	$d_{90} Initial$	1.653	1.546
	$d_{90} Final$	3.107	2.629

Table 5.3: Comparison of solid model with experimental test results
* All the dimensions are in mm. ** Strain values are dimensionless

The accuracy of the solid element models was also measured by triaxiality in all stress states. The triaxiality of all solid element models was plotted against their respective failure strains. All solid models were validated with theoretical triaxiality values which can be seen in the Figure 5.14. The uni-biaxial test (involving complex stress states) also indicated the correct triaxiality at failure with 0.667.

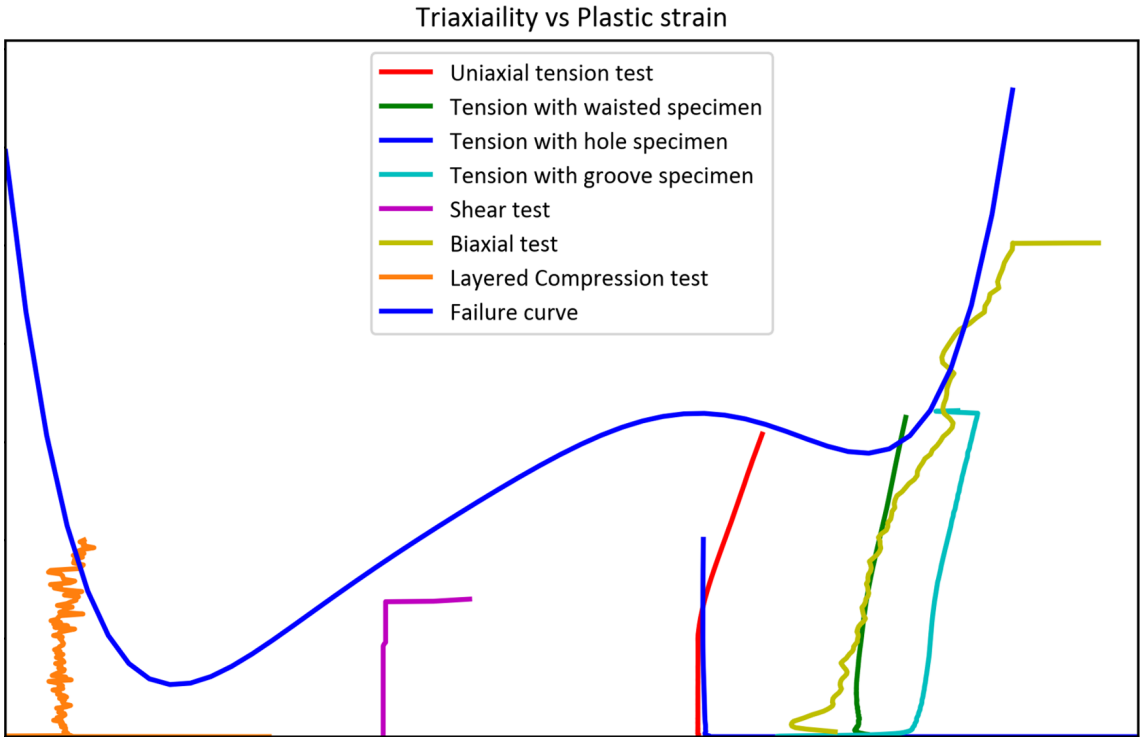

Figure 5.14: Triaxiality vs Failure strain

5.2 Full scale model

A calibrated material card (*MAT_24+GISSMO) was tested on a full vehicle level to verify the accuracy and robustness of the calibrated material model in a complex load case. The frontal Offset Deformable Barrier (ODB) crash test case Figure 5.15 was chosen, where the car was driven at 64 km/h with 40% of the vehicle overlap on a deformable barrier. This test is challenging in terms of structural crashworthiness, as a limited portion of the vehicle structure gets engaged during the crash exposing occupants to higher injury risks mostly due to the risk of structural failure of passenger compartment.

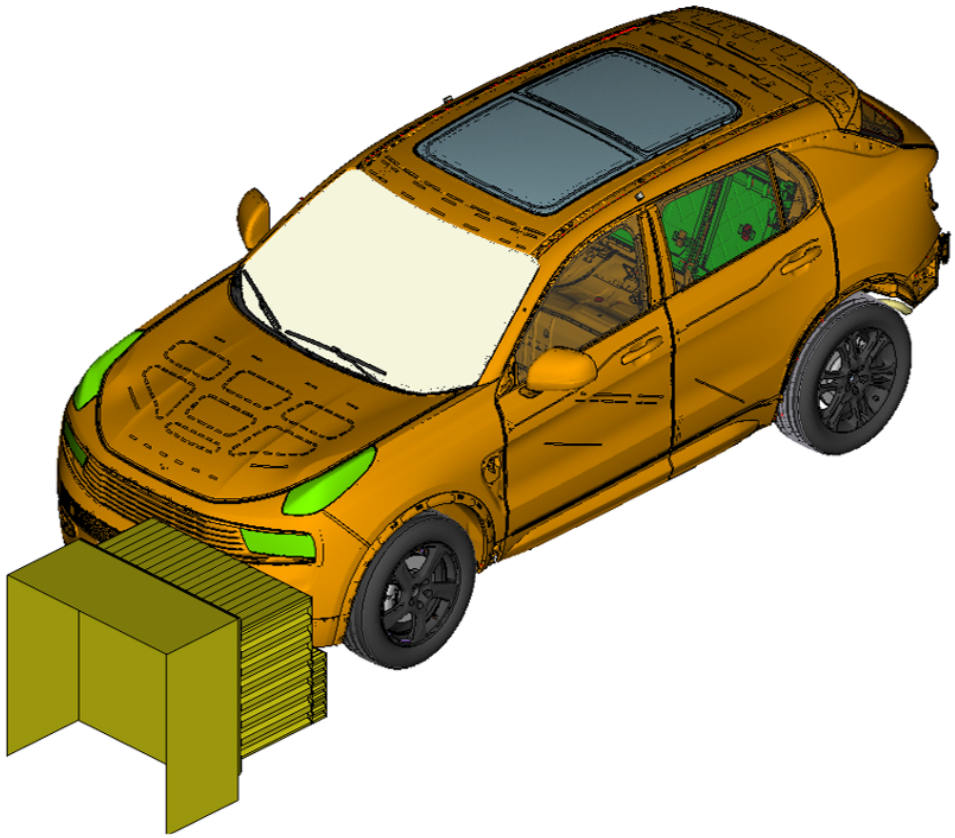

Figure 5.15: ODB crash test

Front side members of the vehicle structure play a vital role in crash management in frontal crashes. The new material card was assigned to the front members of Lynk & Co 01 vehicle for validation. Two tests were conducted, one with *MAT_24+GISSMO assigned to the front side members and another with CrachFEM.
Figures 5.16 and 5.17 illustrate the BIW of Lynk & Co 01 pre and post deformation, respectively. Both models were superimposed to check the deviation in deformation behaviour by visual inspection. Similar deformations were observed in both the cases. This indicates that the front side members of the vehicle structure, assigned with different material models exhibited similar performance during the crash. Detailed deformation of BIW front end are observed in Figure 5.17.

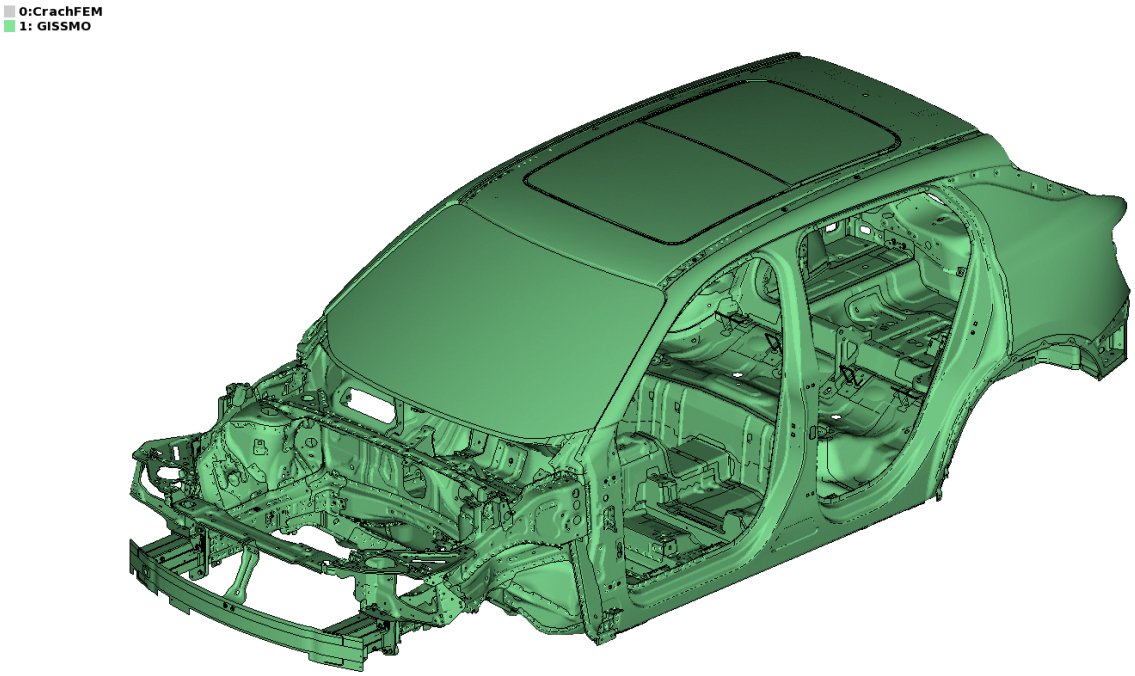

Figure 5.16: BIW

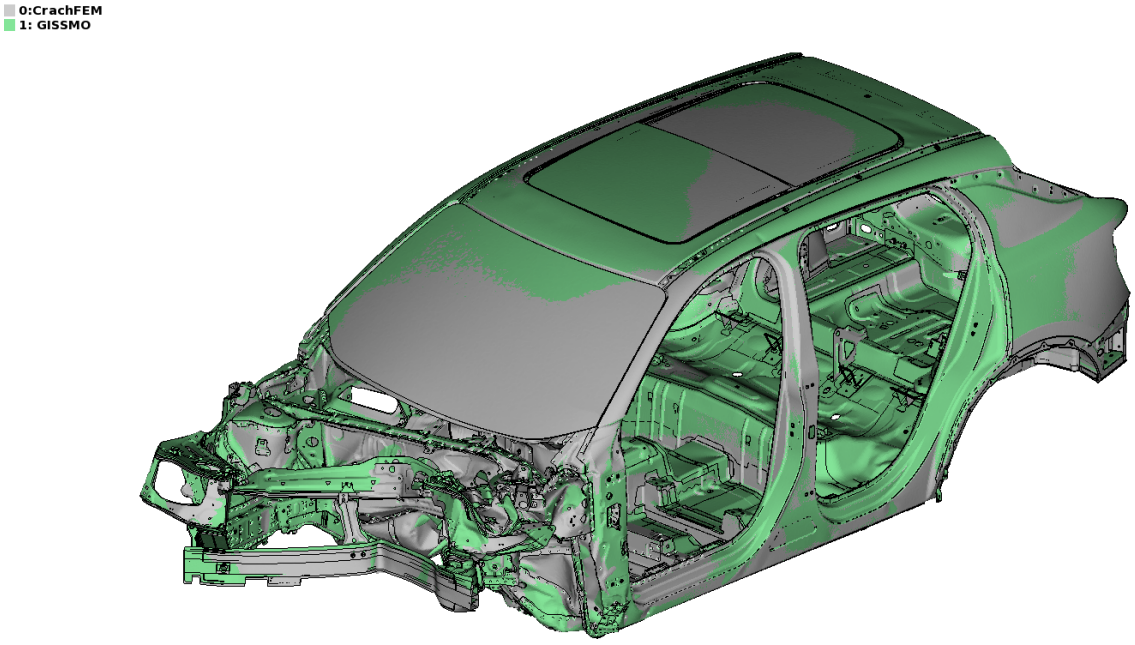

Figure 5.17: BIW deformed

A closer observation of the front side members of the vehicle structure are shown in the below figures (Fig. 5.18, Fig. 5.19, Fig. 5.20, Fig. 5.21, Fig. 5.22, Fig. 5.23). The left side members of the vehicle structure were engaged in the test and the bending modes between the two tests were found to be similar and this is observed in the Figure 5.19. This indicated the calibrated material card (*MAT_24+GISSMO) was in good agreement with CrachFEM that can also be justified by the section

forces in the side member and can be viewed in the Figures 5.22 and 5.23.

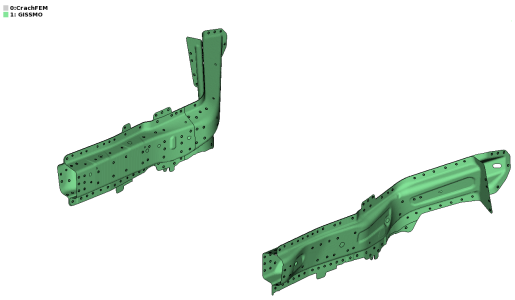

Figure 5.18: Front side member

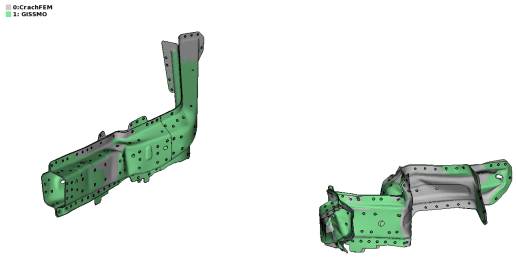

Figure 5.19: Deformed Front side member

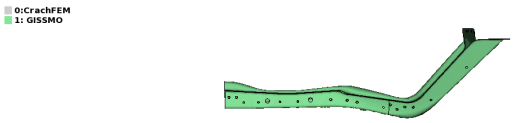

Figure 5.20: Front side member

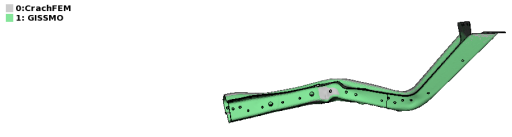

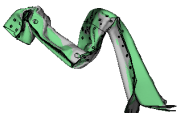

Figure 5.21: Deformed Front side member

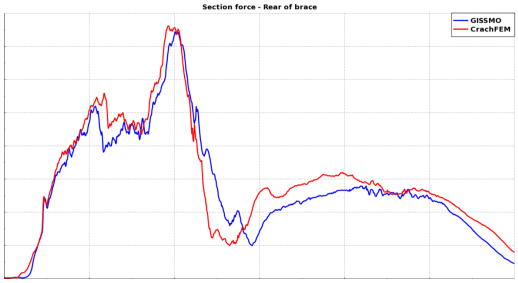

Figure 5.22: Section force - brace

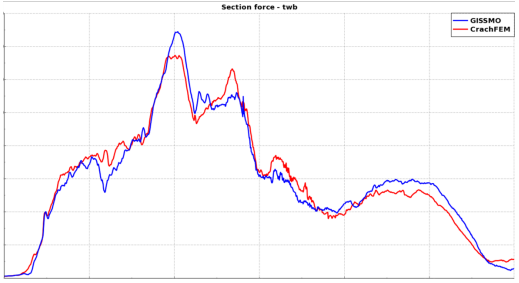

Figure 5.23: Section force - TWB

6

Conclusion

The primary focus of this study was to develop a virtual test laboratory and methodology to characterise the material in different stress states. Calibration of any material card required detailed data collection from extensive experimental tests which are time consuming and expensive. A new approach was outlined in this study, where an optimisation based method demonstrated the feasibility of capturing material behaviour in different stress states using a single hardening curve obtained from a uniaxial tension test. The optimisation technique using the response surface method was found to be more efficient in extrapolating the hardening curve of the material using a solid element specimen. The solid element models developed in this study showed promising results in capturing the failure behaviour similar to that of experimental test results. A quantitative result accuracy of 94.5% was achieved using the solid test specimens in comparison with the physical tests. This was observed for the particular cases of triaxiality and crack dimensions.

The method of extracting the maximum data from the solid element models was a key step in calibrating a GISSMO material definition. The parameters like triaxiality, failure strain, and critical strain values were carefully chosen from the results obtained from the solid element models. Extensive optimisation played a vital role in tuning the parameters like DMGEXP (Damage Exponent), FADEXP (Fading stress exponent), LCSDG (Curve: Triaxiality v/s failure strain), ECRIT (Critical plastic strain), and EPSF (Plastic failure strain) in GISSMO card. Mesh regularisation was done for the GISSMO damage model so that the failure strain was scaled over a mesh range of 0.5 mm to 5 mm. A calibrated GISSMO card with *MAT_24 was found to be very effective in predicting the failure of material in different stress states. Most complex stress states like biaxial test and bending test were accurately captured with this method.

The calibrated material card (*MAT_24+GISSMO) was also tested on a full vehicle model to test its accuracy in a complex load case. The results from the ODB crash test revealed that the deformation behavior and section forces in the front side member of the vehicle was found to be quite similar when GISSMO and CrachFEM material models were used. Hence the calibrated material card was in good agreement with CrachFEM. The methodology outlined here significantly led to the reduction in the computational time and was found to be cost-effective. The proposed approach clearly illustrated that a single hardening curve from a uniaxial tension test led to the complete calibration of material model with good correlation with experimental data. Hence the huge cost of material testing could be minimised. Another advantage of this method was its consistency and repeatability, as the same methodology holds good for other grades of steel and the virtual test laboratory developed in this thesis consisting of eight different specimens could be used for the comprehensive development and calibration of material and damage models.

7
Future Scope

The provided methodology and results obtained were promising for the given material and also constitute a fixed framework in the development and calibration of necessary material models from the tensile test. Since the behavior of the material was versatile and varies with their properties, in the future factors like strain rate and lode parameters could be included in the above-mentioned methodology. Over the last few years, polymers have played a vital in automotive applications, hence this methodology could also be evaluated for the characterisation of polymers.

In the current method, the flow curve was calibrated using a uniaxial tension test whereas the flow curve might be calibrated for complex stress states i.e bend test or biaxial test using the test data. Also, different sampling methods during the optimisation process may be used to get optimum samples closer to the experimental data. The reliability of the material model (developed using this current method) should also be verified against weld failure analysis.

Manufacturing histories may be included in the damage model to consider the effect of the manufacturing process on the material properties. Other damage models like DIEM, e-GISSMO could be coupled with different constitutive material models (*MAT_33,*MAT_36E, *MAT_37 etc.) and verified (in terms of both time and accuracy). Finally, a potential toolbox could be designed to automate the current methodology, where a calibrated material model is obtained within a few steps.

Bibliography

[1] J C Kraemer, S Bonnet, "CAE Methods in Automotive Industry: Overview of the stakes and prospects", 29th International Congress and Ehibition on Noise Control Engineering.

[2] Yoshio Kojima ,"Mechanical CAE in automotive design: Review", RD Review Toyota CRDL , Vol. 35, No.4

[3] "Structure Simulation" tecosim.com, https://www.tecosim.com/services/structure-simulation (accessed October. 18, 2019)

[4] World Steel Association,The white book of steel.(2012). ISBN 978-2-930069-67-8.Available:https://www.worldsteel.org/en/dam/jcr:7b406f65-3d94-4e8a-819f-c0b6e0c1624e

[5] Stuart Keeler, Menachem Kimchi, Advanced High Strength Steels Application Guidelines Version 6.0, (2017).

[6] S R Singh, S V Shreedhara, "CAE modelling of cast aluminium in automotive structures" Master Thesis, Division of Solid Mechanics, Department of Management and Engineering ,Linköping University, Linköping, Sweden. [Online]. Available: http://liu.diva-portal.org/smash/get/diva2:1372065/FULLTEXT01.pdf

[7] Filipe Andrade, Markus Feucht, André Haufe, "On the prediction of material failure in LS-DYNA: A comparison between GISSMO and DIEM" ,13th International LS-DYNA Users Conference, 2014

[8] J. Lemaitre and J.-L Chaboche. Mechanics of Solid Materials. Cambridge University Press, 1990

[9] J. Lemaitre, A Course on Damage Mechanics,ISBN:978-3-642-18255-6,Springer-Verlag Berlin Heidelberg,1996

[10] Heidi P. FeigenbaumYannis F. Dafalias, "Directional distortional hardening in metal plasticity within thermodynamics", International Journal of Solids and Structures 44, 7526–754, 2007

[11] Niels Saabye Ottosen and Hans Petersson, Introduction to the Finite Element Method. ISBN:0-13-473877-2. 1992

[12] Niels Saabye Ottosen and Matti Ristinmaa, The Mechanics of constitutive modelling. Elsevier Inc, 2005

[13] Klaus-Jürgen Bathe,Finite Element Procedures, 2nd ed, ISBN:978-0-9790049-5-7 ,Pearson Education, Inc,2016

[14] T R Chandrupatla, A D Belegundu , Introduction to finite elements in engineering, 3rd ed, ISBN:0-13-061591-9, Pearson Eduction Ltd.

[15] G E Dieter,Jr., Metallurgy and Metallurgical Engineering series, Mc-graw-Hill Book Company.1961

[16] Robert Basan,Tea Marohnić ,Development of evolutionary procedures for characterization of biological tissues,Research project, University of Rijeka,October 1 2015. behavior BIOMAT

[17] Oscar Bjorklund ,"Ductile failure in High Strength Steels", PhD dissertation, Division of Solid Mechanics, Department of Management and Engineering ,Linköping University, Linköping, Sweden. ISBN: 978-91-7519-389-2

[18] Hjalmar Sandberg,Socar Rydholm ,"Evaluation of material models to predict material failure in LS-DYNA" Master's Dissertation,Division of Solid Mechanics, Department of Construction Sciences, Lund University,Lund, Sweden.

[19] Won Y Yang, Wenwu Cao, Tae-Sang Chung, and John Morris. Applied numerical methods using MATLAB. John Wiley Sons, 2005.

[20] Bradley N Maker, David J Benson, 'Modal Methods for transient dynamic analysis in LS-DYNA',7th International LS Dyna Users Conference

[21] Jonas Gozzi, Plastic Behavior of Steel- Experimental investigation and modelling, PhD dissertation, Division of Structural Engineering - Steel Structures, Department of Civil and Environmental Engineering ,Luleå University of Technology, Luleå, Sweden. ISSN: 1402-1757

[22] Tobias Erhart, 'Review of solid element formulations in LS-DYNA',LS DYNA Forum 2011, Stuttgart 12

[23] Mayank Kumar Singh, Application of steel in automotive industry, International Journal of Emerging Technology and Advanced Engineering,Volume 6, Issue 7, ISSN:2250-2459

[24] André Haufe, Markus Feucht,Frieder Neukamm, Paul DuBois, 'Recent Enhancements to the GISSMO Failure Model in LS-DYNA',European LS-DYNA Conference-Strasbourg,2011

[25] André Haufe, Markus Feucht,Frieder Neukamm, Paul DuBois, 'GISSMO – Material Modeling with a sophisticated Failure Criteria',LS-DYNA Developer Forum,2011

[26] Mikael Schill, Ductile material failure in LS-DYNA ,A seminar on material modelling -DYNAMORE NORDIC.

[27] Kjell Mattiasson, JohanJergéus, PaulDuBois, "On the prediction of failure in metal sheets with special reference to strain path dependence" International Journal of Mechanical Sciences 88, 175-191, 2014

[28] LS-DYNA® KEYWORD USER'S MANUAL, VOLUME I, LS-DYNA R10.0, October 16,2017.

[29] LS-DYNA® KEYWORD USER'S MANUAL, VOLUME II, LS-DYNA R10.0, October 16,2017.

[30] MF GENYld+CrachFEM USER'S MANUAL-Theory,4.2.0, May 22,2014.

8

Appendix 1

8.1 Supporting results

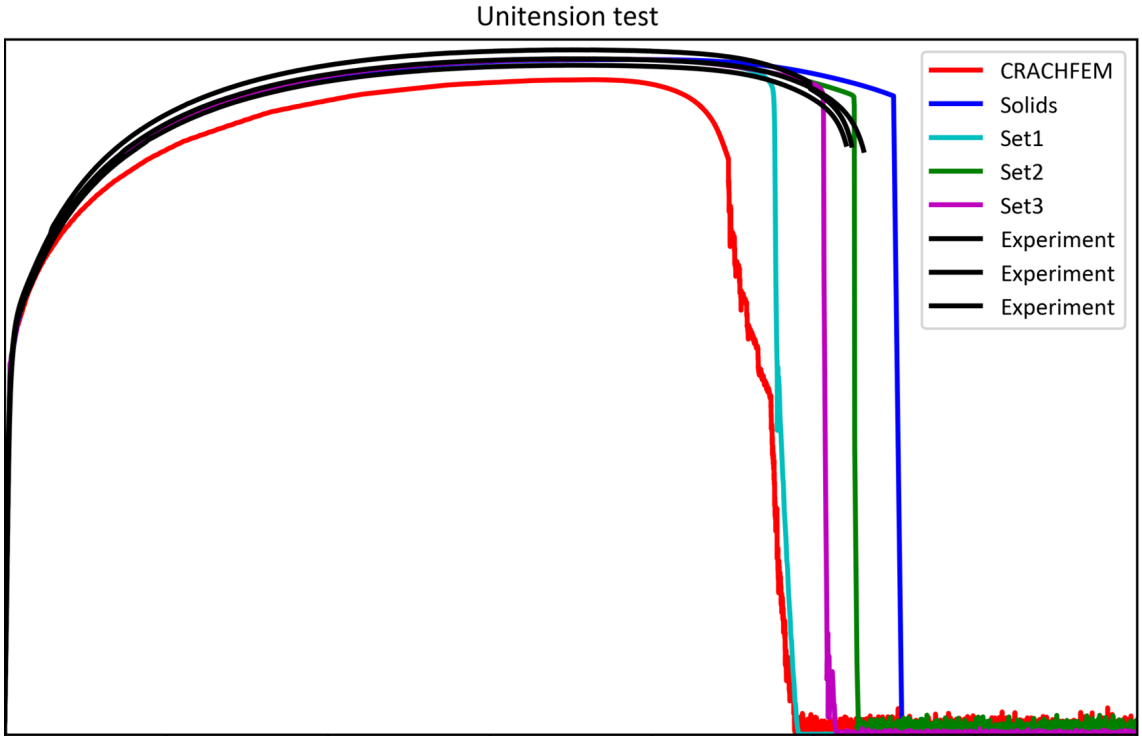

Figure 8.1: Uniaxial test

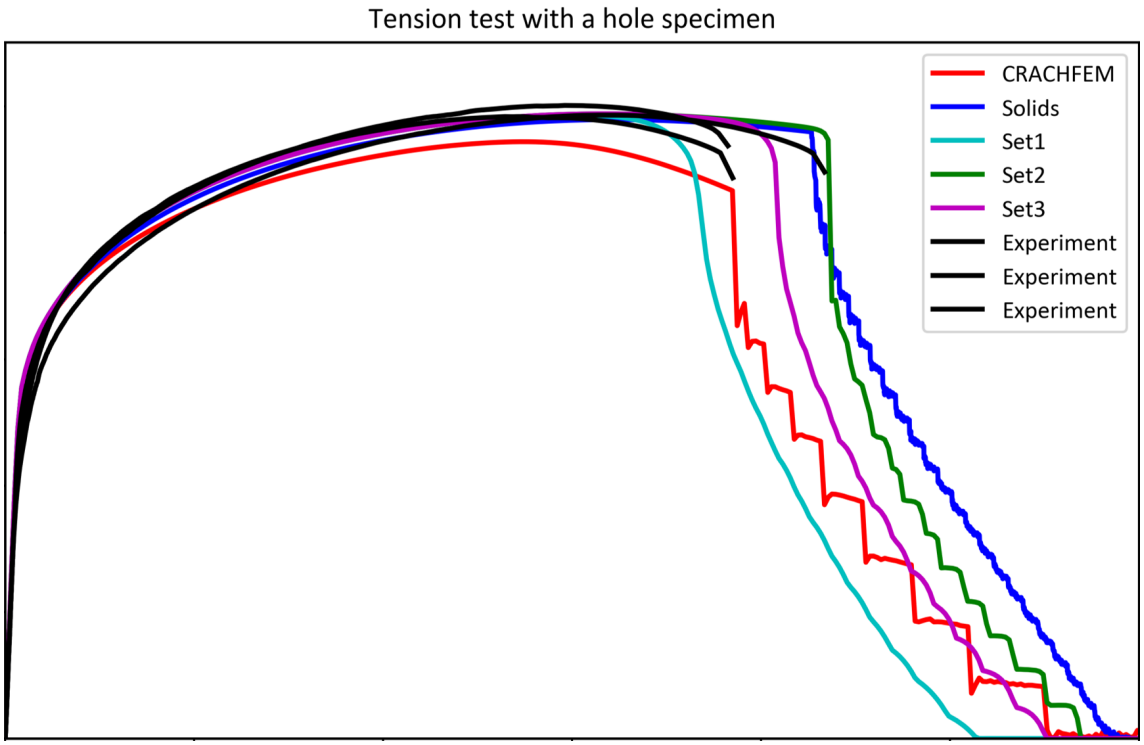

Figure 8.2: Tension test(specimen with a hole)

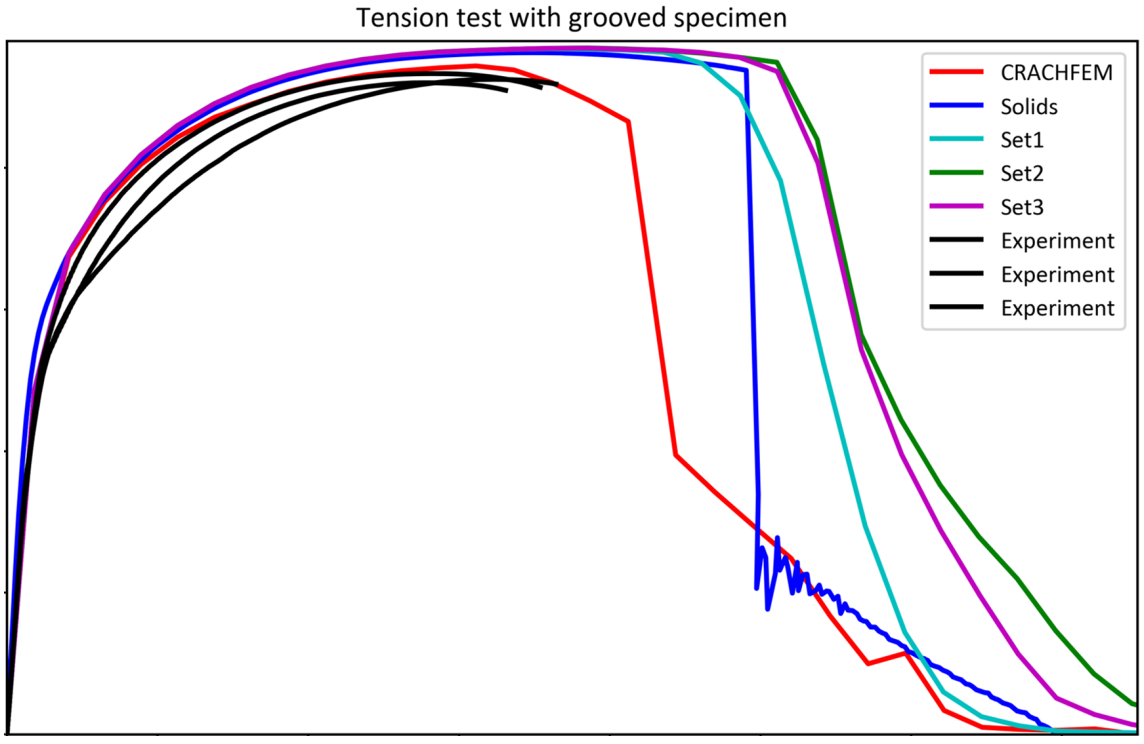

Figure 8.3: Tension test(specimen with a 90°groove)

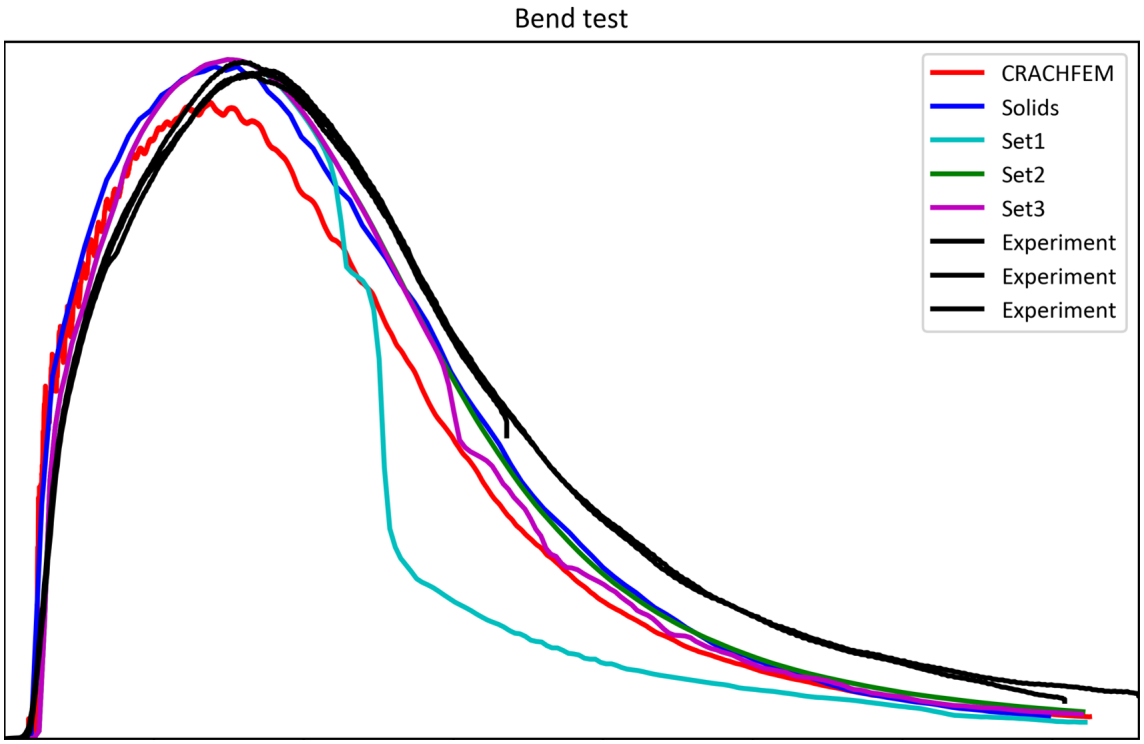

Figure 8.4: Bend test

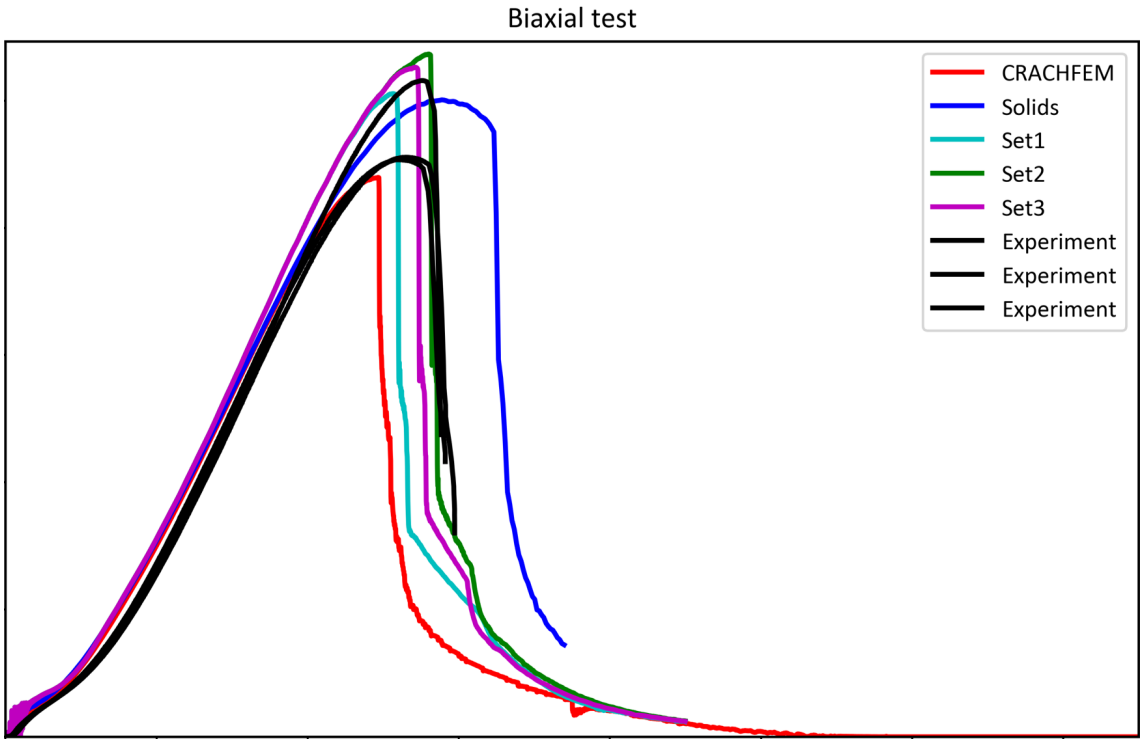

Figure 8.5: Unibiaxial test

8.2 Post failure images

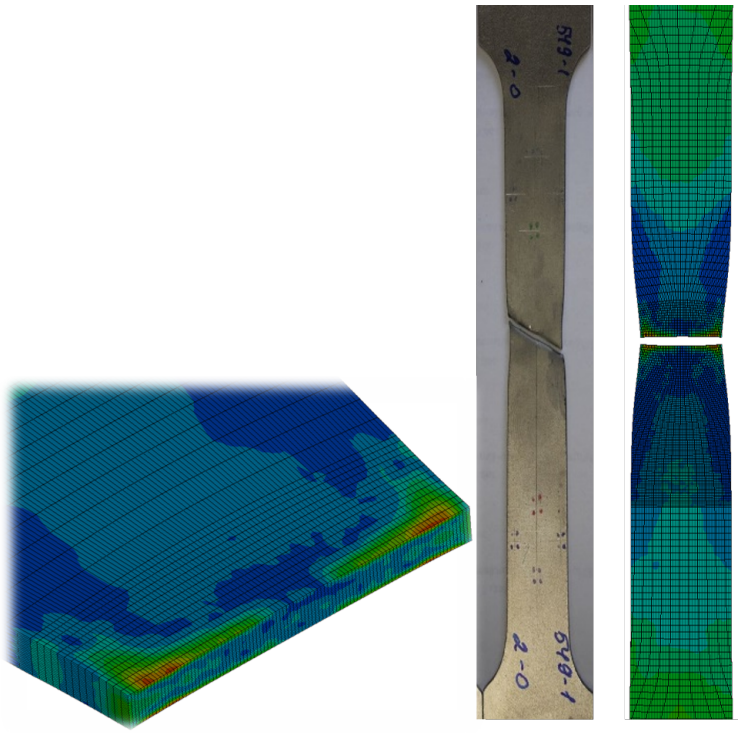

Figure 8.6: Tensile test

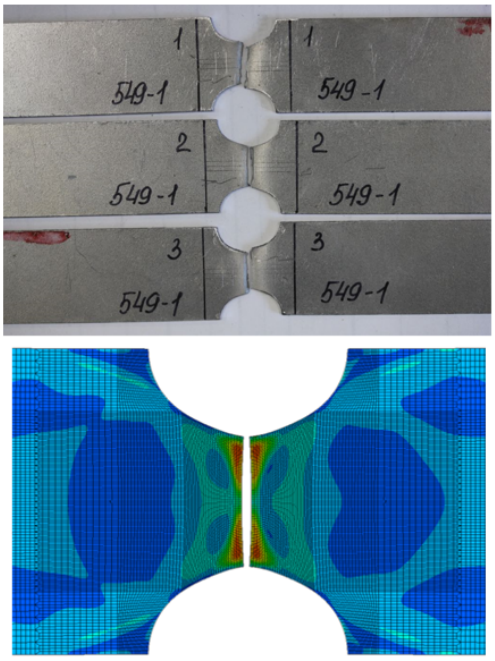

Figure 8.7: Tensile specimen with waist

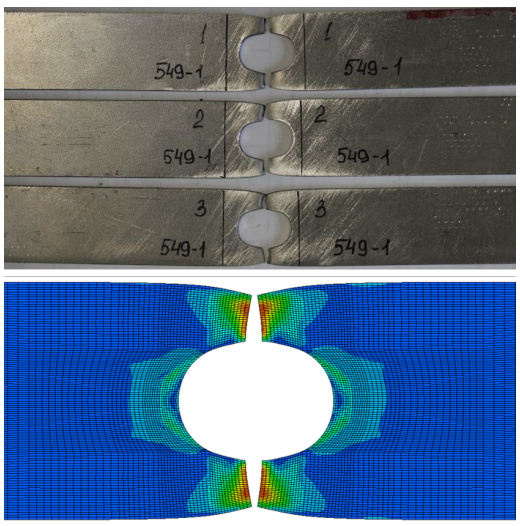

Figure 8.8: Tensile specimen with hole

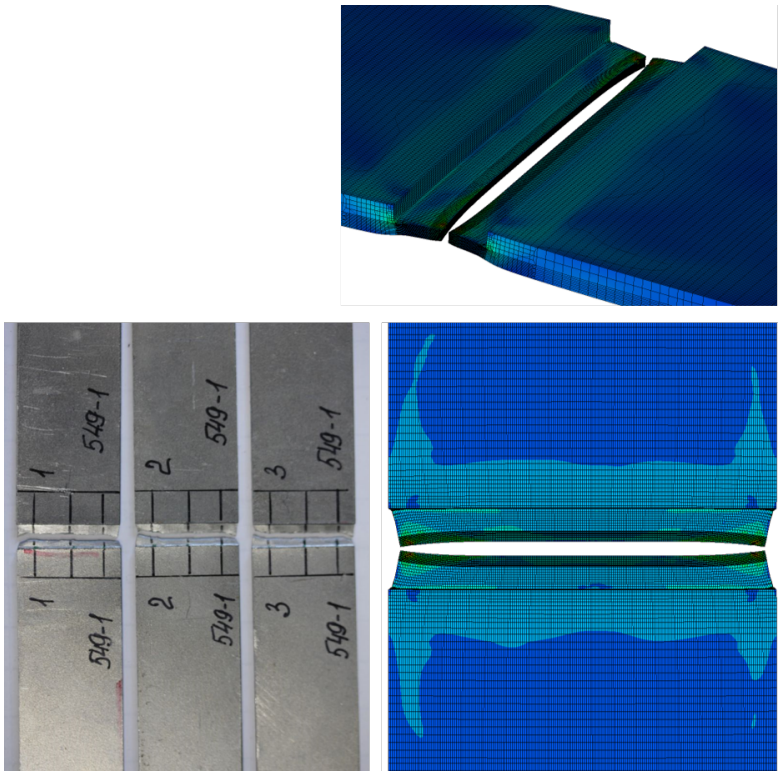

Figure 8.9: Tensile specimen with a groove

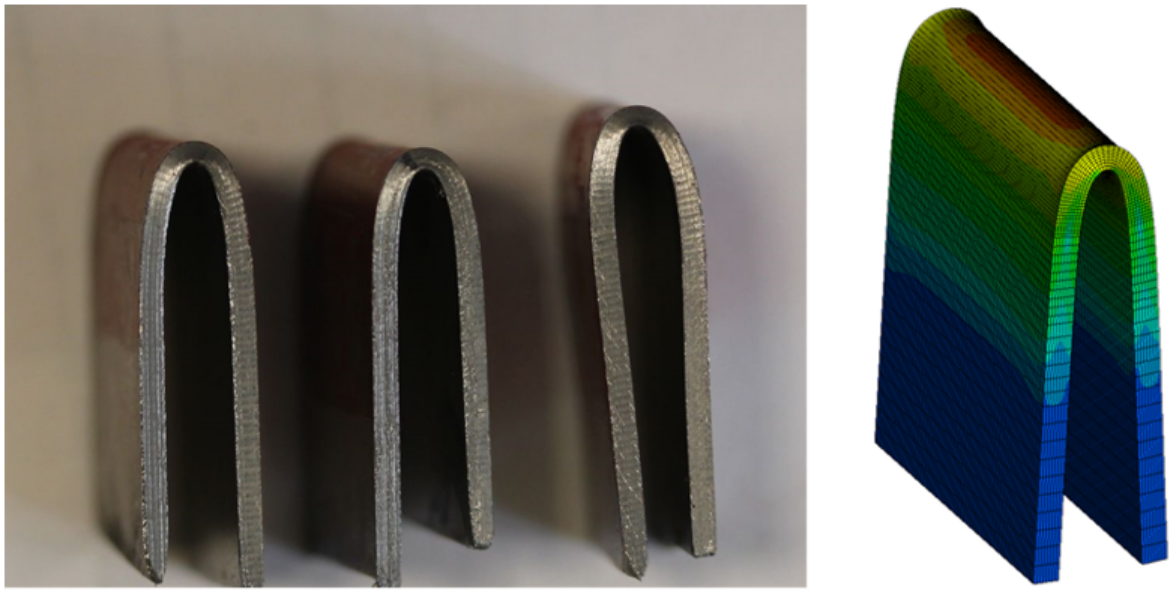

Figure 8.10: Bending test

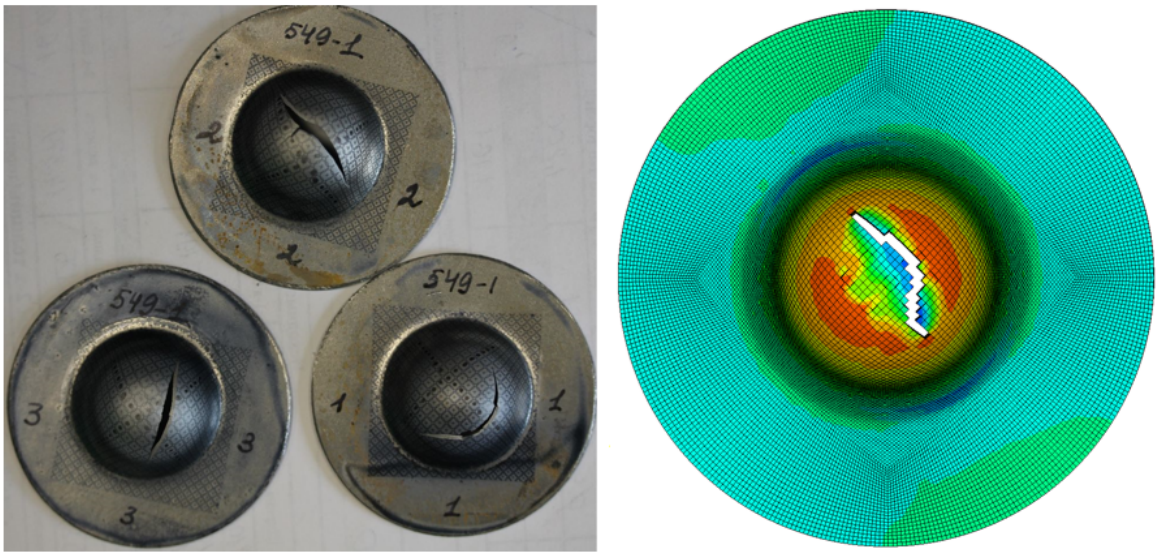

Figure 8.11: Unibiaxial test

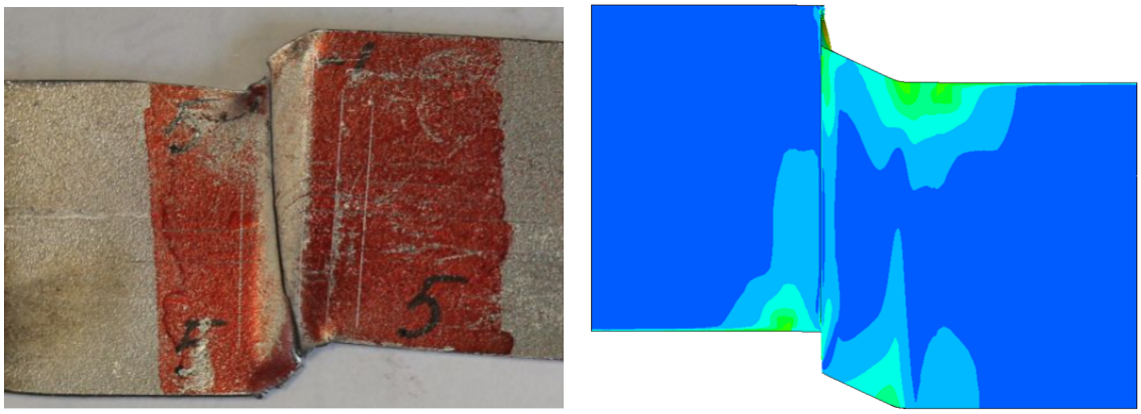

Figure 8.12: Shear test

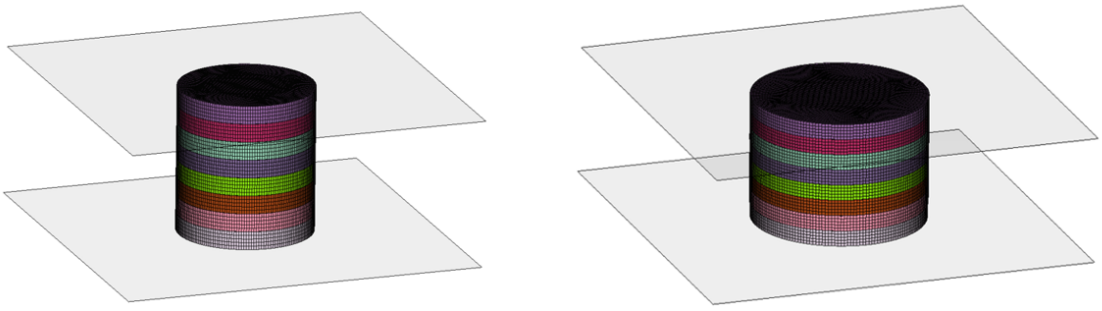

Figure 8.13: Compression test